Computational Functions in Biochemical Reaction Networks

Adam Arkin*‡ and John Ross*
*Department of Chemistry and ‡Department of Neurobiology, School of Medicine, Stanford University, Stanford, CA 94305 USA

ABSTRACT In prior work we demonstrated the implementation of logic gates, sequential computers (universal Turing machines), and parallel computers by means of the kinetics of chemical reaction mechanisms. In the present article we develop this subject further by first investigating the computational properties of several enzymatic (single and multiple) reaction mechanisms: we show their steady states are analogous to either Boolean or fuzzy logic gates. Nearly perfect digital function is obtained only in the regime in which the enzymes are saturated with their substrates. With these enzymatic gates, we construct combinational chemical networks that execute a given truth-table. The dynamic range of a network's output is strongly affected by "input/output matching" conditions among the internal gate elements. We find a simple mechanism, similar to the interconversion of fructose-6-phosphate between its two bisphosphate forms (fructose-1,6-bisphosphate and fructose-2,6-bisphosphate), that functions analogously to an AND gate. When the simple model is supplanted with one in which the enzyme rate laws are derived from experimental data, the steady state of the mechanism functions as an asymmetric fuzzy aggregation operator with properties akin to a fuzzy AND gate. The qualitative behavior of the mechanism does not change when situated within a large model of glycolysis/gluconeogenesis and the TCA cycle. The mechanism, in this case, switches the pathway's mode from glycolysis to gluconeogenesis in response to chemical signals of low blood glucose (cAMP) *and* abundant fuel for the TCA cycle (acetyl coenzyme A).

INTRODUCTION

Biochemical reaction networks (BRNs), such as glycolysis and the tricarboxylic acid cycle, are an integral part of the machinery by which an organism maintains itself and adapts to its environment. These networks are responsible for numerous cellular tasks including the maintenance of homeostasis and the creation and propagation of chemical signals such as those indicating hunger or satiation. It is often very difficult to determine the underlying logic of the regulation of even relatively small portions of a BRN. First, the sub-network may be highly interconnected and contain many feedback loops, branching pathways, etc. Second, it is difficult to determine all the kinetic parameters that determine the behavior of a BRN in vitro let alone in vivo (Fersht, 1985). Third, the great range of temporal and spatial scales over which a large BRN can react to the perturbation of its variables makes it difficult to deduce the laws of biological control and signal processing from examination of models of the dynamic equations of motion (Acerenza, Sauro, and Kacser, 1989). Therefore, it is desirable to develop additional techniques for the investigation of reaction mechanisms, their control and signal processing.

In previous papers we have demonstrated the implementation of formal logical computations and functions such as logic gates, neural networks, and universal Turing machines (Hjelmfelt and Ross, 1992, 1993, 1994; Hjelmfelt et al., 1991, 1992, 1993) by means of macroscopic kinetics of chemical reaction networks. (This work is briefly reviewed under Implementation of Computation with Macroscopic Chemical Kinetics.) The simplest chemical kinetic mechanism capable of computation discussed in these networks bears a striking resemblance to parts of many important multi-enzymatic pathways found in metabolism. It is natural, therefore, to look for logical computation performed by these structures within the known BRNs.

Received for publication 16 March 1994 and in final form 18 May 1994.
Address reprint requests to Dr. John Ross, Department of Chemistry, Stanford University School of Medicine, Stanford, CA 94305. Tel.: 415-723-9203; Fax: 415-723-4817; E-mail: ross@chemistry.stanford.edu.

0006-3495/94/08/560/19 $2.00

Abbreviations used: GCP, glucose carrier protein; G Dg, glucose degradation; GK, glucokinase; HK, hexokinase; G6Pase, glucose-6-phosphatase; PHI, phosphohexose isomerase; PFK1, phosphofructokinase-1; F16BPase, fructose-1,6-bisphosphatase; PFK2, phosphofructokinase-2; F26BPase, fructose-2,6-bisphosphatase; α-GP DH, α-glycerol phosphate dehydrogenase; α-GP Dg, α-glycerol phosphate degradation; TPI, triose phosphate isomerase; GAPDH, glyceraldehyde phosphate dehydrogenase; PGK, phosphoglycerate kinase; PGM, phosphoglycerate mutase; PyrK, pyruvate kinase; PyrC, pyruvate carboxylase; PEPCK, phospho enolpyruvate carboxykinase; LacDH, lactose dehydrogenase; Lac Dg, lactose degradation; CarbA, carbonic anhydrase; Cit1 Dg, cytosolic citrate degradation; PyrDHC, pyruvate dehydrogenase complex; CitSyn, citrate synthase; ICDH, isocitrate dehydrogenase; GluDH, glutamate dehydrogenase; 2-KGDHC, 2-ketoglutarate dehydrogenase complex; SuccDH, succinate dehydrogenase; MalE, malic enzyme; MalDH, malate dehydyrogenase; AspTA, aspartate transaminase; AlaTA, alanine transaminase; AK, adenylate kinase; OAA, oxalacetate;Glu, glutamate; Ala, alanine; Suc, succinate; Cit, citrate; AsP, aspartate; Pyr, pyruvate; PEP, phosphoenolpyruvate; CoA, coenzyme a; ACoA, acetyl-coenzyme A; Gluc, glucose; G6P, glucose-6-phosphate; F6P, fructose-6-phosphate; F16BP, fructose-1,6-bisphosphate; F26BP, fructose-2,6-bisphosphate; ℄, catalytic subunit of cAMP-dependent protein kinase; DHP, dihydroxyacetone phosphate; GAP, glyceraldehyde phosphate; 3PGA, 3-phosphoglyceraldehyde; 13DPGA, 1,3-diphosphoglyceraldehyde; 23DPGA, 2,3- diphosphoglyceraldehyde; 2PGA, 2-phosphoglyceraldehyde; α-GP, α-glycerol phosphate; LAC, lactate; HIP, Hexose-phosphate Interconversion Pathway; sHIP, simplified HIP. In these models, when a chemical species, such as citrate, may take on different concentrations in different cellular spaces (i.e., the extracellular space, cytosol, and mitochondrion) its abbreviation is postfixed with a number designating the compartment to which it belongs (0, 1, and 2 respectively).

The purpose of the present work is first to demonstrate, by way of calculations based on macroscopic kinetic equations, that enzymatic biochemical reaction mechanisms can perform computational functions. We do so in a sequence of studies: in the section titled Models of BRNs, we show that plausible models of enzymatic reaction mechanisms and networks of such mechanisms can realize logic functions such as AND, NOT, OR, and exclusive OR (XOR) gates. One of these mechanisms is a radical simplification of the hexose-phosphate interconversion pathway (sHIP) in glycolysis/gluconeogenesis, wherein the complex, experimentally determined rate laws are replaced with Michaelis-Menten forms. It is shown that this mechanism, operating in isolation from the rest of the metabolic pathway, can function analogously to an AND gate. Choices of the kinetic parameters determine the range of operating behavior from a nearly classical Boolean AND gate (Horowitz and Hill, 1984) to a generalized fuzzy-logic function (Klir and Folger, 1988). For nearly all choices of the parameters, however, the mechanism retains a basic AND functionality.

Second, we show, again by calculations, that parts of established biochemical reaction pathways can perform computational functions. A more representative model of the HIP mechanism is constructed by using rate laws culled from the literature (see Analysis of a Portion of Glycolysis). This pathway involves the interconversion of fructose-6-phosphate (F6P) between its two bisphosphate forms, fructose-1,6-bisphosphate (F16BP) and fructose-2,6-bisphosphate (F26BP) (Stryer, 1988). The bicyclic enzymatic loop may function as a switch that selects either the degradative or the biosynthetic mode of the pathway. We examine the properties of this mechanism in isolation from the rest of glycolysis/gluconeogensis (the HIP model). In this case, no material flows into or out of the hexose-phosphate pool so that the total concentration of the three fructose-phosphate forms is a constant. In addition, the concentrations of each of the adenosine phosphates are assumed to be held constant by buffering. We find that the steady state of the mechanism, parameterized by the concentrations of cAMP and cytosolic citrate, functions as an asymmetric fuzzy aggregation operator with properties akin to a fuzzy AND gate.

The section titled Analysis of a Portion of Glycolysis Embedded in a Large Metabolic Model describes the placement of the HIP mechanism within a complex model of glycolysis/gluconeogenesis (GG) coupled to the tricarboxylic acid (TCA) cycle (the GGTCA model) and material flows into and out of the hexose phosphate pool. We show that the fructose-phosphate interconversion mechanism may act as a category of logic gate with respect to input from cAMP and cytosolic citrate; the direction of flux changes from glycolytic to gluconeogenic only when blood glucose is low *and* there is no need of intermediates for the TCA cycle to drive respiration. In both the HIP and GGTCA model, the steady-state concentration of F6P as a function of cAMP and cytosolic citrate exhibits a logical structure similar to that of the isolated HIP mechanism, i.e., it is an asymmetric fuzzy aggregation operator akin to the fuzzy AND gate.

MATERIALS AND METHODS

All calculations were constructed in the C programming language interfaced to the Numerical Algorithms Group, Ltd. (Oxford, UK, Release Mark 15) FORTRAN library. The numerical integration of the kinetic equations was achieved by the routine D02NBF, a variable step-size integrator applicable to stiff sets of ordinary differential equations. The steady state for a system of equations is defined as the point at which none of the dynamic variables change more than 0.1%/1000 time units. The unit of time is dependent on the formulation of the system of equations. In the HIP and GGTCA models, for example, this time unit is equal to 1 min. All calculations were executed on a DECstation 3100 workstation.

We obtained rate laws for the various enzymatic reaction mechanisms derived from Michaelis-Menten, steady-state, King-Altman, or derivative procedures (Fersht, 1985). As such, the resultant kinetic networks are valid only on the slow (near steady-state) manifold of the network (Roussel and Fraser, 1993). It is assumed that neglecting the transient response of the network has little effect on its logical structure and that the concentration of thermodynamically unfavorable enzyme-ligand complexes is negligible.

IMPLEMENTATION OF COMPUTATION WITH MACROSCOPIC CHEMICAL KINETICS

Prior work

In previous studies, we began with an abstract reaction mechanism in which the species, A_j and B_j, are, for example, an active and inactive form of an enzyme respectively (Hjelmfelt and Ross, 1992; Hjelmfelt et al., 1991, 1992). Such mechanistic motifs are found in many biological systems; for example, Fig. 1 shows a phosphorylation/dephosphorylation cycle similar in structure to the mechanism in Fig. 2 of Hjelmfelt et al. (1991) and Fig. 1 of Okamoto et al. (1988), which is important in glycolysis/gluconeogenesis. If such a mechanism is driven far from equilibrium, then the stationary state of, let us say A_j, varies sharply from a low value to a high value as the catalyst concentration, C_j, is changed (see Fig. 2 of Hjelmfelt et al., 1991). This behavior is equivalent to a McCulloch-Pitts neuron (McCulloch and Pitts, 1943) (Okamoto, 1992; Okamoto et al., 1988a, b, 1989). This formal neuron is a simple thresholding device that changes state between 0 and 1 at a given value of an input variable.

We then proceeded to couple such reaction mechanisms by postulating an enzyme E_{ji} that converts A_j (for an excitatory connection) or B_j (to achieve an inhibitory connection) to the catalyst for a different chemical neuron designated by the index i. By considering such connections of two chemical neurons to a third, we constructed logic gates (AND, OR, NOR, and others) (Hjelmfelt et al., 1991). For example, the output of a chemical neuron AND gate is high if and only if the outputs of the two input neurons are high. Networks of these chemical logic gates were used to construct a finite state machine, stacks, a universal Turing machine and neural networks. This work constitutes the chemical implementation of neural networks.

In further work we proceeded to show that mass-coupled continuous stirred tank reactors, each containing a bistable

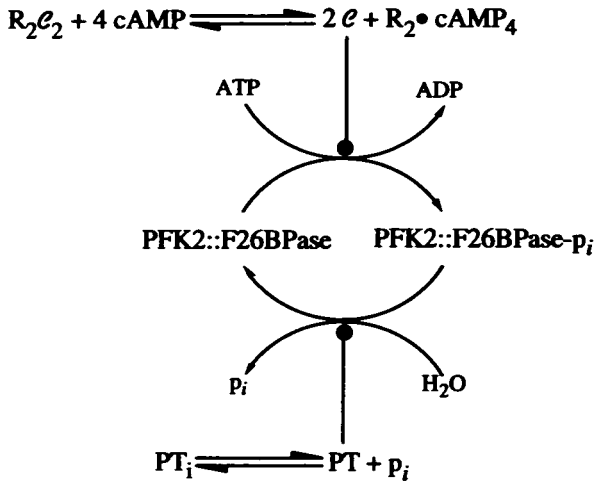

FIGURE 1 A diagram of the phosphorylation/dephosphorylation cycle of the tandem enzyme PFK2::F26BPase. The lines ending in filled circles indicate that $\mathscr{C}$ and PT are catalysts for the phosphorylation and dephosphorylation reactions, respectively. This mechanism has a reaction topology very similar to Fig. 2 in (Hjelmfelt et al., 1991). Here, $R_2\mathscr{C}_2$ represents the tetrameric enzyme, cAMP-dependent protein kinase. R denotes the regulatory subunit and $\mathscr{C}$ denotes the catalytic subunit. PT denotes a generic phosphatase which is inhibited by the presence of inorganic phosphate. The inactive phosphatase is denoted by PT_i. The activity of the PFK2 moiety of the tandem enzyme is reduced by phosphorylation whereas that of the F26BPase is increased. This figure is similar to Fig. 1 of (Schacter et al., 1984b).

chemical reaction, can serve as a pattern recognition device (Hjelmfelt and Ross, 1993, 1994; Hjelmfelt et al., 1993). The tanks are coupled through mass-transfer tubes, and their transfer coefficients are determined from a Hebbian learning rule derived from the pattern to be recognized by the system (Hjelmfelt et al., 1993). Further, we have shown that pattern recognition, chaos, and multistability may occur in mass-coupled excitable systems (Hjelmfelt and Ross, 1994). In this case the computational functions and pattern recognition are accomplished during the transient excursion of the system in concentration space rather than the arrival at a stationary state. Thus, the system accomplishes computations quite differently from the usual neural networks.

One of the main purposes of such studies is related to the study of chemical reaction mechanisms. If chemical reaction mechanisms running far from equilibrium may perform computational functions, then we may inquire whether in well-known reaction mechanisms computational functions occur and, if they do, what role and purpose they serve.

Applicability of logic to BRNs

The description of biochemical dynamics employing Boolean logic is not new. Following the discovery of the operon control of genetic transcription and allosteric enzyme regulation (both of which may exhibit a steep sigmoidal response in the activity of the gene or enzyme with respect to the concentration of a specific chemical species) a number of attempts were made to assign logic levels to the sigmoidal activity responses of the cooperative enzymes. Monod and Jacob (1961), Sugita (1963), Kauffman (1969, 1971), and Thomas (1973), for example, all tried to formulate genetic control problems in terms of Boolean networks. Slightly later, Glass and Kauffman (1973) proposed a logical analysis of nonlinear biochemical control networks. Employing a specific mapping of the continuous system to a discrete binary system, they predicted, partially, the global qualitative dynamics (e.g., the presence of multiple stationary states, oscillations, etc.) of the original system of equations.)

The mechanism in Hjelmfelt et al. (1991) was developed to serve as a chemical switch that may be used to control information (chemical concentrations and fluxes) in a computational network. Many enzymatic mechanisms involved in the regulation of homogeneous metabolism exhibit a skeletal structure similar to this theoretical scheme. Fig. 1 is an example of such a mechanism (and is used in the models described in the sections titled Analysis of a Portion of Glycolysis and Analysis of a Portion of Glycolysis Embedded in a Large Metabolic Model). Here, the activity of the tandem enzyme phosphofructokinase-2::fructose-2,6-bisphosphatase (PFK2::F26BPase) is regulated by phosphorylation and dephosphorylation by cAMP-dependent protein kinase and a phosphatase, respectively. Such phosphorylation cycles are common in metabolic regulation (Schacter et al., 1984a, b). The phosphorylation cycle in Fig. 1 exhibits steady-state behavior reminiscent of the formal chemical neuron despite the more complex kinetics of the interconversion. Fig. 2 shows a computer simulation of the steady-state concentrations of phosphorylated and native PFK2::F26BPase as a function of the concentration of the catalytic subunit of protein kinase, $\mathscr{C}$. Compared with the transition of the chemical neuron in Fig. 2 of Hjelmfelt et al., (1991), the transition between the low and high steady states of the protein species is relatively smooth; this effect will be discussed in more detail later. Given that the interconversion of two

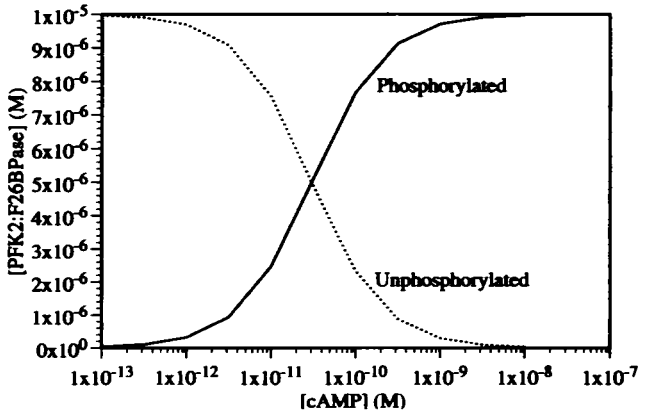

FIGURE 2 Plot of the steady state levels of phosphorylated and unphosphorylated PFK2::F26BPase (Fig. 1) as a function of the concentration of the catalytic subunit of protein kinase, $\mathscr{C}$. The transition between low and high concentrations of the phosphorylated protein is gradual unlike the formal neuron described in (Hjelmfelt et al., 1991). The kinetics for this system are taken from reference (Schacter et al., 1984b).

chemical species by essentially irreversible, multiply affected, reciprocal enzyme reactions is a pervasive motif in biochemical control, it is natural to begin to analyze extended biochemical networks in light of the work described briefly above in the preceding section.

MODELS OF BIOCHEMICAL REACTION NETWORKS

In this section we introduce and analyze a series of enzymatic reaction mechanisms in order of increasing complexity. We show, by numerical calculation of the solution of their deterministic (macroscopic) rate equations, that these mechanisms are capable of supporting well-defined computational functions.

Implementation of logic functions by single-enzyme mechanisms

A step toward a formal description of biochemical computational functions such as switches is the formulation of the internal dynamics in terms of familiar enzyme kinetics. A very simple mechanism with two substrates and a single regulated enzyme is sufficient to realize any of the standard logic functions, AND, OR, XOR (exclusive or), etc. A schematic for an enzymatic logic gate is

$$A^* \xrightarrow{E_1} B \rightarrow P^* \tag{1}$$

where the chemical species A^*, the substrate for enzyme E_1, is held constant by a buffered flow and produces the species B that is degraded to a product P^*. All species bearing an asterisk superscript are considered to be held constant. In the following calculations we assume that the degradation is accomplished by an enzyme with simple Michaelis-Menten kinetics. There is a single differential equation describing the time-dependence of the only dynamic variable of the system, B,

$$\frac{dB}{dt} = \nu_1 - \nu_2 \tag{2}$$

where ν_1 and ν_2 are the rates of the reactions catalyzed by enzyme E_1 and the degradation process, respectively. We may realize a (two-input) logic gate by: 1) defining the concentration of B to be the output of the gate; 2) hypothesizing two external effectors (inputs) of E_1, denoted by I_1 and I_2; 3) defining the rate of the conversion of B to P^* to be described by simple Michaelis-Menten kinetics; and 4) constructing an enzymatic rate law for E_1 that provides a functional realization of the desired logic. The following mechanisms for E_1 demonstrate this construction for AND, OR, and XOR gates.

Enzyme Kinetics:

$$\begin{array}{ccccccc} E_1 & \xleftrightarrow{n \cdot I_1} & E_1 I_{1_m} & & & & \\ \Big\updownarrow {\scriptstyle m \cdot I_2} & & \Big\updownarrow {\scriptstyle m \cdot I_2} & & & & \\ E_1 I_{2_m} & \xleftrightarrow{n \cdot I_1} & E_1 I_{1_m} I_{2_m} & \xleftrightarrow{A} & E_1 I_{1_m} I_{2_m} A & \xrightarrow{k_{cat}} & E_1 I_{1_m} I_{2_m} + B \end{array}$$

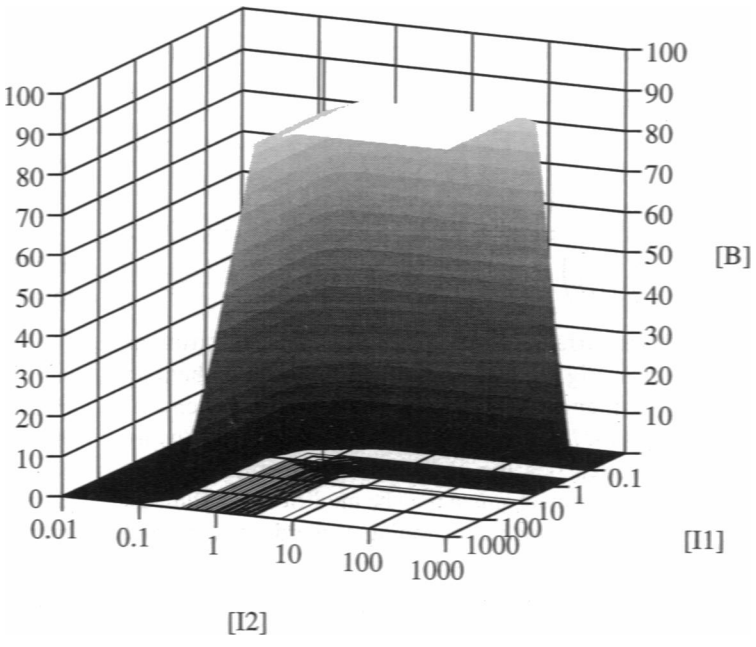

FIGURE 3 A specification of the kinetics of enzyme E_1 from Eq. 1 and a plot of the surface of the steady-state concentration of B calculated from the integration of Eq. 2. All concentrations are in arbitrary units (designated simply as "units"). Here, and in all the other three-dimensional plots in this paper, a contour plot of the steady-state surface appears on the base of the graph. The parameters for ν_1 *are:* $V_{max} = 1.1$ units/s, $K_S = 35.0$ units, $K_{I_1} K_{I_2} = 1.0$ units, $n = m = 3.0$. The parameters for ν_2 *are:* $V_{max} = 1.0$ units/s, $K_S = 50.0$ units. The concentration of the output species, B, changes from its basal to its maximal value over the range when both I_1 and I_2 change from less than 0.3 to more than 3.0 units. This mechanism may be considered to function as an AND gate. Note that this gate is fully symmetric with respect to binding of both inputs.

Consider the catalytic scheme shown in Fig. 3 where the terms above and to the right of the ↔ symbol (denoting rapid equilibria) represent the binding of input species or substrate to the appropriate enzyme complex. In the equations given below it is assumed (but not necessary) that the dissociation constants for a given species from any of the enzyme complexes to which it may bind are all equal. Thus, the dissociation constant, K_{I_1}, is the same whether I_1binds to E_1 or to E_1I_{2m}. This mechanism realizes an AND gate because both activators I_1 and I_2 are necessary for the catalytic activity of E_1. The rate law for this mechanism, with the assumption of rapid equilibrium for the binding of substrate and effectors to the various enzyme complexes, is given by

$$\nu_1 = k_{cat}[EI_{1_n}I_{2_m}A] = \frac{V_{max}[A]}{K_S\left(1 + \left(\frac{K_{I_1}}{[I_1]}\right)^n + \left(\frac{K_{I_2}}{[I_2]}\right)^m + \left(\frac{K_{I_1}}{[I_1]}\right)^n\left(\frac{K_{I_2}}{[I_2]}\right)^m\right) + [A]} \quad (3)$$

where k_{cat} is a first-order rate constant, V_{max} is defined as k_{cat} times the total concentration of E_1, and K_s is the dissociation constant of A from $E_1I_{1n}I_{2m}$. A plot of the surface of the steady-state concentration of B as a function of I_1 and I_2 is shown in Fig. 3. In this system, the concentration of B is proportional to the activity of E_1 relative to that of the degradation process. It should be noted that in this mechanism we assume the concentrations of $E_1I_{1n}A$ and $E_1I_{2m}A$ to be negligible. In fact, the thermodynamic barrier to the binding of A to E_1I_{1n} (E_1I_{2m}) can only be higher than that for binding to $E_1I_{1n}I_{2m}$by an amount equal to the Gibbs free energy of binding of m (n) molecules of I_2 (I_1) to the E_1I_{1n} (E_1I_{2m}) complex. We make similar assumptions in the other enzyme mechanisms considered.

The OR gate is easily implemented by constructing an enzyme mechanism in which two different activators compete for the same binding site in the enzyme. With the assumption of a simplistic sequential mechanism we get the mechanism shown in Fig. 4. for which the rate law is

$$\nu_1 = k_{cat}([EI_{1_n}A] + [EI_{2_m}A]) = \frac{V_{max}\left(1 + \left(\frac{K_{I_1}}{[I_1]}\right)^n\left(\frac{[I_2]}{K_{I_2}}\right)^m\right)[A]}{\left(1 + \left(\frac{K_{I_1}}{[I_1]}\right)^n + \left(\frac{K_{I_1}}{[I_1]}\right)^n\left(\frac{[I_2]}{K_{I_2}}\right)^m\right) \times (K_S + [A])}. \quad (4)$$

The resultant surface of the steady-state concentration of B is shown in Fig. 4. An example of another mechanism that may implement an OR gate has two independent binding sites for I_1 and I_2 and the substrate can bind to any enzyme complex bearing at least one activator.

Finally, the last mechanism may be modified to include an $E_1I_{1n}I_{2m}$ complex incapable of binding A in order to construct an XOR gate. In this case, simultaneously high concentrations of the effectors favors the formation of the inactive doubly bound form. The kinetic reaction mechanism is shown in Fig. 5 for which we have the rate law

$$\nu_1 = k_{cat}([EI_{1_n}A] + [EI_{2_m}A]) \quad (5)$$

$$\nu_1 = \frac{V_{max}\left(1 + \left(\frac{K_{I_1}}{[I_1]}\right)^n\left(\frac{[I_2]}{K_{I_2}}\right)^m\right)[A]}{\mathscr{A} + \mathscr{B}}$$

where

$$\mathscr{A} = K_S\left(1 + \left(\frac{K_{I_1}}{[I_1]}\right)^n + \left(\frac{[I_2]}{K_{I_2}}\right)^m + \left(\frac{K_{I_1}}{[I_1]}\right)^n\left(\frac{[I_2]}{K_{I_2}}\right)^m\right)$$

$$\mathscr{B} = [A]\left(1 + \left(\frac{K_{I_1}}{[I_1]}\right)^n\left(\frac{[I_2]}{K_{I_2}}\right)^m\right).$$

The corresponding surface of steady-state concentrations of B is shown in Fig. 5. The mechanism behaves analogously to a classical XOR gate except that at intermediate concentrations of both inputs there is significant deviation of [B] from its basal value. This may be minimized by the choice of the equilibrium constant between the single-activator and double-activator complexes (calculations not shown). For simplicity, in this model, this constant was chosen to be the same as the binding of a single activator to the unbound enzyme.

These mechanisms are not, of course, the only way of realizing these logic functions with a single multiply affected enzyme but are merely representative. Further, the steepness of the transition from low to high steady-state concentrations of B in all these mechanisms is accomplished using a high degree of cooperativity ($n = m = 3.0$ in Figs. 3–5). If a lower degree of cooperativity is used, the functionalities are maintained, but the transition region is much more gradual. For example, a surface of steady states created using the mechanism from Eqs. 1 and Fig. 3 but where $n = m = 1.0$ has much the same shape as that in Fig. 3 and thus it retains its AND gate function, but the transition from low to high [B] is far less steep (data not shown). As discussed below, although the steepness of the transition may affect the absolute output concentrations of networks that include this gate, the qualitative behavior of the network is unchanged. In the next section we demonstrate, among other things, how a steep response may be obtained without resorting to high cooperativity in the binding of effector to an enzyme.

Implementation of logic functions by multi-enzyme mechanisms

The construction of logic devices by macroscopic kinetics is not limited to the mechanisms of single enzymes; such devices with computational functions may be distributed throughout a kinetic reaction mechanism made up of many enzymes. The locus of control in these systems is distributed among different proteins instead of being located on a single enzyme. This type of control is thus "allos-enzymic" in analogy to the allosteric control of the kinetics of a single enzyme. Consider the mechanism shown in Fig. 6. It is similar in form to a portion of glucose metabolism known to be

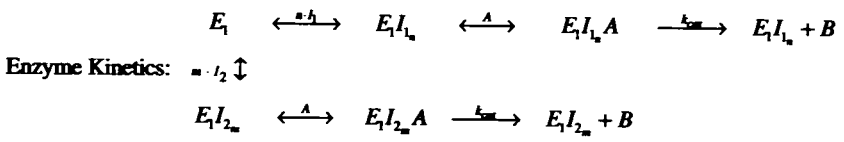

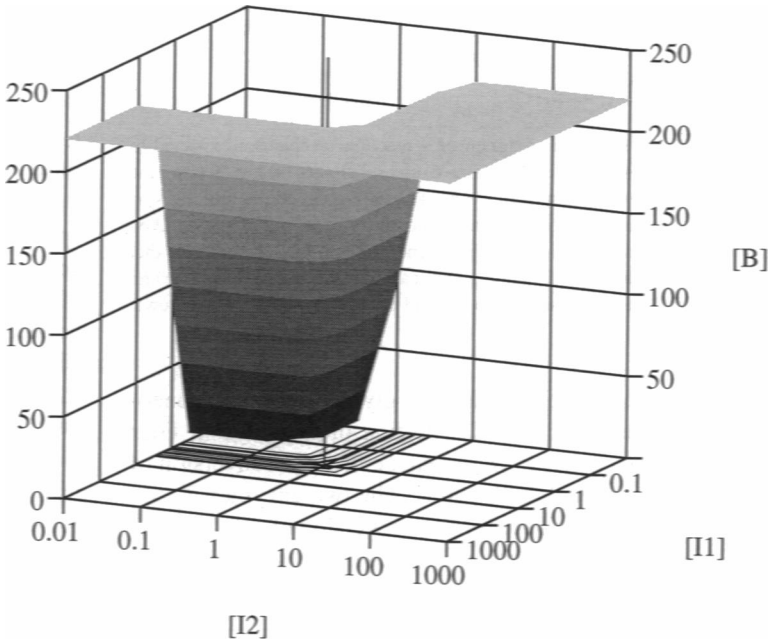

FIGURE 4 A specification of the kinetics of enzyme of E_1 from Eq. 1 and a plot of the surface of steady-state concentration of B calculated from the integration of Eq. 2. The parameters for ν_1 are: $V_{max} = 1.1$ units/s, $K_S = 35.0$ units, $K_{I_1} K_{I_2} = 1.0$ units, $n = m = 3.0$, the parameters for ν_2 *are:* $V_{max} = 1.0$ units/s, $K_S = 50.0$ units. The transition region in this gate occurs over the same range as in Fig. 3 except that only one *or* the other input need be within this interval.

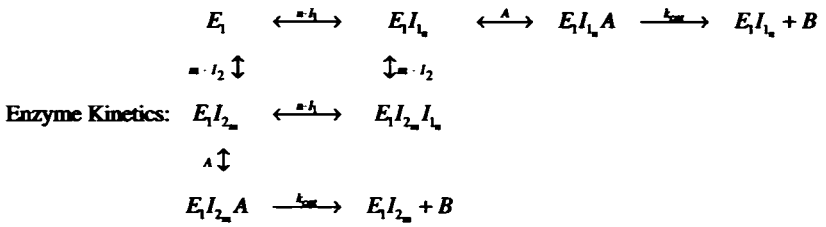

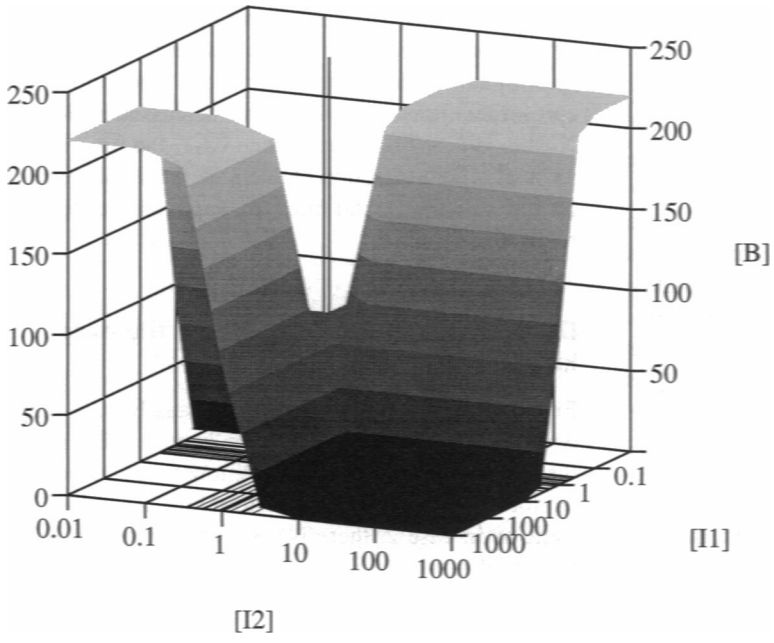

FIGURE 5 A specification of the kinetics of enzyme of E_1 from Eq. 1 and a plot of the surface of steady-state concentration of B calculated from the integration of Eq. 2. The parameters are the same as in Fig. 4. Here, the output species is only high when one and only one of the input species is above the transition threshold (between 0.3 and 3.0 units). The moderate increase in B when both I_1 and I_2 are approximately equal to 1 unit is a result of the choice of the equilibrium constants for the binding of I_1 or I_2 to EI_{2_m} or EI_{1_n} respectively.

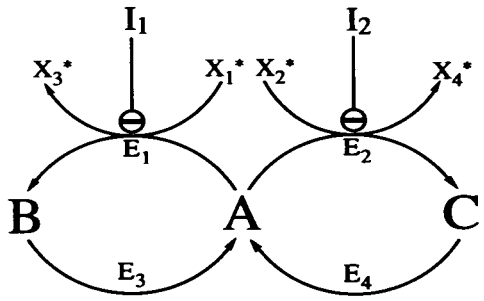

FIGURE 6 A schematic diagram of a reaction mechanism expected to function as an AND gate. *A*, *B* and *C* are substrates or products of the reactions catalyzed by enzymes E_1–E_4. Two non-competitive inhibitors, I_1 and I_2 are considered to function as inputs to the gate; the output is taken to be *A*. The lines ending in open circles enclosing minus signs indicate that I_1 and I_2 are inhibitors of E_1 and E_2. The reactants denoted by X's (here and in Figs. 8 and 9) are considered to be held constant by buffering or flows.

involved in the switching between glycolytic and gluconeogenic flux (see Analysis of a Portion of Glycolysis). Four irreversible enzymes, E_1–E_4, catalyze the interconversion of three species labeled *A*, *B*, and *C*. The two enzymes E_1 and E_3, which are responsible for the conversion of *A* to either *B* or *C* are inhibited by two external chemical species, I_1 and I_3. Consider the case where the reactions follow Michaelis-Menten kinetics and the inhibition is noncompetitive. The time evolution equations are given by

$$v_1 = \frac{V_{max_1}[A]}{(1 + [I_1]/K_{I_1})(K_{S_1} + [A])}$$

$$v_2 = \frac{V_{max_2}[A]}{(1 + [I_2]/K_{I_2})(K_{S_2} + [A])} \qquad (6)$$

$$v_3 = \frac{V_{max_3}[B]}{K_{S_3} + [B]} \qquad v_4 = \frac{V_{max_4}[C]}{K_{S_4} + [C]}$$

$$\frac{d[B]}{dt} = v_1 - v_2 \qquad \frac{d[C]}{dt} = v_3 - v_4 \qquad (7)$$

$$[A] = S_{tot} - [B] - [c] \qquad (8)$$

where v_1–v_4 are the rates of the reactions catalyzed by the respective enzymes E_1–E_4, I_1 and I_3 are inhibitors, and $S_{tot} = [A]+[B]+[C]$ is a constant. All the enzyme rate laws are assumed to be irreversible. In real enzyme systems, there is always at least a small backward reaction. In closed systems, this small component forces the steady-state concentrations of the substrates to a ratio dependent on their standard Gibbs free energies. However, the assumption of irreversibility is good if the enzyme reactions are driven by coupling to other "buffered" chemical species. The reactions catalyzed by E_1 and E_2 are considered to be coupled to external species (X_1 and X_2) in this way. Because the concentrations of the buffered species remain constant during the experiment, the system is formally open but the effects of these reactants are absorbed into the kinetic constants, V_{max} and K_m, of the rate laws v_1 and v_2. We confirmed by explicit calculations (not shown here) that the addition of small backward fluxes to the four enzyme reactions does not significantly alter the shape of the surface of steady-state concentrations of the three substrates (*A*, *B*, and *C*).

This mechanism may function as a logical AND gate. The inhibitor concentrations are the two inputs to the gate, and the concentration of *A* is the output. When no inhibitors are present, the steady-state concentrations of *A*, *B*, and *C* are equivalent. When one or the other inhibitor is present, material is apportioned between *A* and one of the other species; thus, *A* assumes a higher steady-state value. Finally, when both inhibitors are present, conversion of *A* to the other two species is blocked, and *A* therefore attains its highest concentration. These responses are reminiscent of the behavior of an AND gate. However, the steepness of the transition between the highest and lowest concentrations of *A*, the absolute values of these concentrations, and the symmetry of the response, depend on the exact kinetic parameters of the enzymes. Calculations of the steady-state concentrations of *A* from integration of Eqs. 6–8 (the mechanism in Fig. 6) result in a plot almost identical to that of Fig. 3 (data not shown). A crisp response is obtained, for example, with the following parameters (case 1): $V_{max_1} = V_{max_2} = 5.0$ units, $V_{max_3} = V_{max_4} = 1.0$ units, $K_{S_1} = K_{S_2} = K_{S_3} = K_{S_4} = 5.0$ units, $K_{I_1} = K_{I_2} = 1.0$ units. All concentrations are in arbitrary units. In this case, the concentration of *A* is virtually constant at less than 1 unit, unless both I_1 and I_2 are present, at above approximately 6 units each, at which point a steep transition to a value greater than 90 occurs. Thus, the mechanism with these parameters functions much like a Boolean AND gate. A much smoother transition is obtained by substituting (case 2): $K_{S_1} = K_{S_2} = K_{S_3} = K_{S_4} = 35.0$ units. Here, there is a relatively smooth transition between the highest and lowest steady-state concentrations of *A* over the range between 1 and 10 units in each of the inputs. Thus, this gate is closer to a fuzzy AND operator. The difference is that in the former case, the binding constants for the substrates *A*, *B*, and *C* were much smaller than any of the (average) concentrations of these species. Thus, the enzymes are functioning within the zero-order ultrasensitivity regime discussed in Goldbeter and Koshland (1981). In the second case, the binding constants are a significant fraction of even the maximal concentrations of the substrates and thus the apparent cooperativity is reduced.

Dependence of functionality on the exact kinetic parameters

Fig. 7, the results of integration to steady state of Eqs. 6–8 with the same parameters as case 2 above with the exception that $V_{max_1} = V_{max_2} = 1.0$ unit, demonstrates an interesting behavior: though the transition from low [*A*] to high [*A*] is the same as in case 2, there is a significant rise in the concentration of *A* when only one or the other inhibitor is present. This is caused by the decrease in maximum activities of E_1

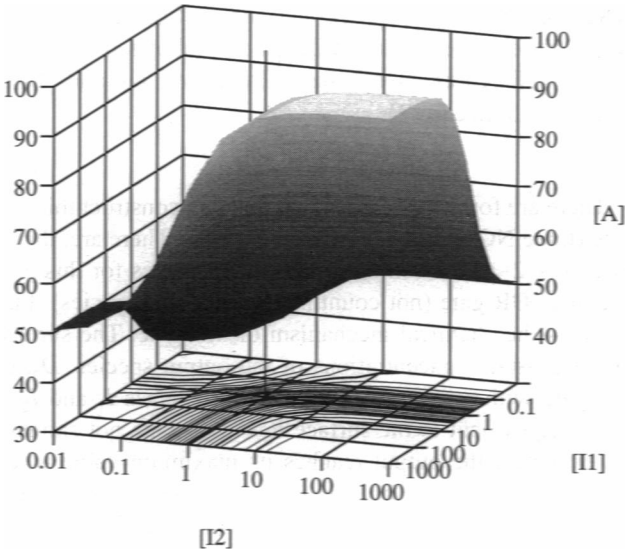

FIGURE 7 Plot of the steady-state surface of A (from Fig. 6) based on integration of Eqs. 6–8. The parameters used are: $V_{max_1} = V_{max_2} = V_{max_3} = V_{max_4} = 1.0$ units, $K_{S_1} = K_{S_2} = K_{S_3} = K_{S_4} = 35.0$ units, $K_{I_1} = K_{I_2} = 1.0$ units. In this case, the reactions converting A to B and C have equivalent maximum velocities to the reciprocal reactions making A. This leads to a commensurately higher basal concentration for A than that obtained in Fig. 3 or from mechanisms in which V_{max_1} and V_{max_2} are greater than V_{max_3} and V_{max_4} respectively. This gate is similar to that in Fig. 3 except the dynamic range is smaller and A attains a value slightly greater than its minimum when only one or the other inhibitor is "ON". This gate has, therefore, both AND-like and OR-like properties. (See Dependence of Functionality on the Exact Kinetic Parameters) The reaction mechanism, with the given parameters, then conforms more to the definition of a fuzzy aggregation operator (see Appendix A) than to a crisp or fuzzy AND gate. The significantly non-zero value of the minimal output concentration make the connection of this gate to other similar gates problematic (see Preservation of Dynamic Range by Input/Output Matching of Coupled Reaction Mechanisms).

and E_2, which convert A to B and C relative to the reverse reactions. Thus, the reaction mechanism with the given parameters exhibits a logical structure somewhat between an AND and an OR gate. If the output, A, of this gate, G_1, were to serve as an input species to another gate mechanism, G_2, then different results are possible. First, we assume the basal output of G_1 is well below dissociation constant, K_{D2}, of A from the regulated enzyme of G_2. Consider the concentration, $A_{1,1}$, of the output of G_1 in the presence of exactly one input. If the concentration of $A_{1,1}$ is significantly below K_{D2} and the output concentration of G_1 in the presence of both inputs, $A_{1,2}$, is significantly above this constant, then this mechanism is for all practical purposes a simple AND gate. If, however, $A_{1,1}$ is a significant fraction of the appropriate dissociation constant, then G_1 may act as an OR gate with respect to its input to G_2. If G_1 is connected to a number of different gates, then G_1 might variously function as an AND, an OR, or something in between. The qualitative function of this mechanism is thus partially dependent on the exact choice of the kinetic parameters in the network. For a physically realistic choice of the kinetic constants governing the mechanism in Fig. 6, the mechanism is constrained to demonstrate a synergetic action between the inputs to the gate. Thus, the steady state of this mechanism will always function as a logical aggregation operator with an AND-like component.

Connections of reaction mechanisms with computational functions

There are two subtly different ways to connect models of biochemical reaction mechanisms that represent different logic gates. For example, two "single-enzyme" mechanisms from the section Implementation of Logic Functions by Single-Enzyme Mechanisms, above, can be connected as follows:

$$\begin{array}{l} A^* \xrightarrow{E_1} B \rightarrow P_1^* \\ \qquad\quad \perp \\ C^* \xrightarrow{E_2} D \rightarrow P_2^* \end{array} \tag{9}$$

or

$$\begin{array}{l} A^* \xrightarrow{E_1} B \xrightarrow{E_3} D \rightarrow P_2^* \\ \qquad\quad \downarrow \\ \qquad\quad P_1^* \end{array} \tag{10}$$

where the symbol $\perp$ in Eq. 9 indicates that B is an effector of E_2. The species B may play the role of effector for another "single-enzyme" gate (Eq. 9) or it may be fed in as a substrate to another computational reaction mechanism (Eq. 10). If B is fed in as a substrate to a subsequent mechanism, then the steady-state concentration of B is directly affected by the activity of E_2 relative to the relevant inputs (to E_2). The differences between substrate and effector connections is an area for further study (see below). There is, perhaps, an electronic analogy that can be made to describe these types of connections: an effector connection uses little power (i.e., it only requires a relatively small change in the concentration of an input chemical to cause a big change in flux through the enzyme and the effector is not degraded by the reaction) and therefore may be compared to a connection of the output of an electronic device to the base of a transistor. On the other hand, a substrate connection is like a switchable current-source or capacitor on the collector of the transistor. Unless the source is turned on, no power will flow through the transistor, and biasing the base will have no effect.

We focus here on networks built with effector connections between separate mechanisms representing logic functions. Networks of this type are analogous to BRNs connected by chemical signaling compounds, such as cAMP, Ca^{2+}, and growth factors, which are not major metabolites but rather serve to activate or inhibit specific receptors or catalysts near or remote from the origin of the signal. The networks described in the section Networks of Enzymatic Reaction Mechanisms Implementing Logic Function are constructed from AND gates based on the mechanism in Fig. 6 and on chemical NOT gates based on the mechanism shown in

Fig. 8. The NOT gate in Fig. 8 is almost equivalent to the chemical neuron discussed above; however, instead of using simple mass-action kinetics, the reaction dynamics are described by rate laws such as those in Eq. 6. The output of the hypothetical biochemical NOT gate, indicated by the concentration of D, is high (low) when the concentration of I_5 is low (high). This is much like the response of unphosphorylated PFK2::F26BPase to cAMP in Fig. 2. Again the transition between the extremal concentrations of D can be steep or gradual with respect to $[I_5]$ depending on the specific choice of the kinetic constants.

An aggregation operator, such as AND, and a complementation operator, such as NOT, are sufficient to express any logic function (Horowitz and Hill, 1984).

Preservation of dynamic range by input/output matching of coupled reaction mechanisms

A connection between, for example, an AND gate and a NOT gate may be implemented by causing the output species of the AND gate to be the inhibitor to the relevant enzyme in the NOT gate. This is not a trivial task because, to preserve the dynamic range of the final output species (say D), the difference between the minimum and maximum concentrations of A should span the transition region of the NOT gate. For example, $[A]$ should span 1–10 units for interface to a NOT gate with the parameters $V_{max_5} = 10.0$ units, $V_{max_6} = 1.0$ unit, $K_{S_5} = K_{S_6} = 5.0$ units, and $K_{I_5} = 1.0$ unit (just as [cAMP] should span the range 0.1 pM and 10 nM to take advantage of the full dynamic range of the phosphorylation cycle in Figs. 1 and 2). This matching can be achieved in a number of ways; for example, fast equilibria placed between the gates can serve as multipliers and dividers of the input concentration. Alternatively, the input species may be coupled (through an effector connection) to intermediate NOT gates (having the appropriate inhibition constants) to produce a mechanism similar to the cyclic cascades used in biological systems for signal amplification (Schacter et al., 1984a).

Networks of enzymatic reaction mechanisms implementing logic functions

Given that matching conditions are met it is simple to construct any combinational logic function from the enzymatic AND and NOT gates discussed above. Consider, for example, the construction of an OR gate (symbolized by $I_1 + I_2$) from AND gates (symbolized by $I_1 \wedge I_2$) and NOT gates (symbolizedby $\bar{I}$):

$$I_1 + I_2 = \overline{(\bar{I}_1 \wedge \bar{I}_2)} \tag{11}$$

There are four "primitive" gates used to construct this OR gate (three NOT gates and one AND gate). There are, therefore, $3 \times 2 + 3 = 9$ internal chemical species for this biochemical OR gate (not counting the buffered species). Fig. 9 shows the chemical mechanism of this gate. The surface of steady-state concentrations of the output species, D_3, of this gate with respect to the two input species I_1 and I_2 is nearly equivalent to the surface in Fig. 4 (data not shown). As expected, the output reaches its maximum value when one, or the other, or both inputs are present in relatively significant amounts (greater than approximately 10 units) and is minimized when neither input chemical is present.

When more complex logic functions are to be realized issues such as matching and specific implementation by "primitive" gates become more important. Consider a network based on the logical equation:

$$I_1 \oplus I_2 = \overline{\overline{(I_1 \wedge \bar{I}_2)} \wedge \overline{(\bar{I}_1 \wedge I_2)}} \tag{12}$$

where "$\oplus$" stands for the XOR operation. This expression

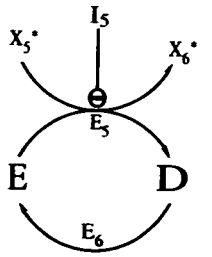

FIGURE 8 A simple NOT gate. The output of the gate is D; the steady-state concentration of D decreases in the presence of I_5. The concentration of all starred species are held constant by buffering or flows.

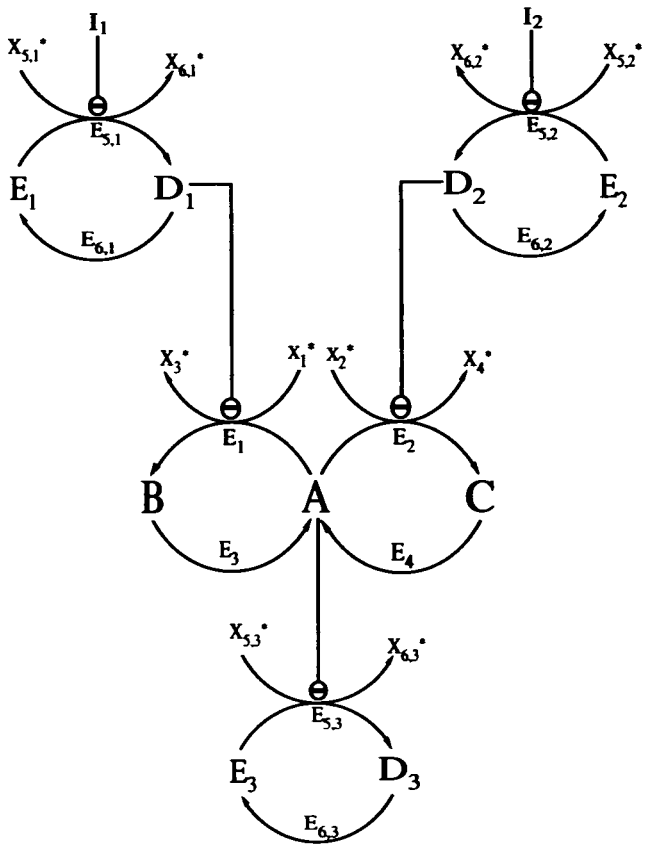

FIGURE 9 The chemical mechanism for the OR gate represented by Eq. 11. There are three separate NOT gates and one AND gate for a total of nine internal species. The output of the gate is the concentration of species D_3.

uses eight gates (for a total of $5 \times 2 + 3 \times 3 = 19$ species). The kinetic constants (inhibition constants, K_Is, and maximum velocities, V_{max}s) of the corresponding network of AND and NOT mechanisms may be chosen, by inspection, to minimize loss of dynamic range. For example, if the parameters for the AND gate are the same as case 1 discussed earlier and the NOT gates have the parameters discussed in the preceding section, then the constituent gate outputs traverse concentrations from those well above to those well below the chosen K_Is of the enzymes. The model, then, exhibits behavior close to the classical XOR function except at the point $I_1 = I_2 \approx 10.0$ units. The high concentration at this point is a result of the slight mismatching between the transition regions of the AND and the NOT mechanisms. A plot of the surface of steady-state concentrations of the final output of this mechanism would look much like Fig. 5.

The XOR function can be realized by another equation:

$$I_1 \oplus I_2 = \overline{(\overline{I_1} \wedge \overline{I_2})} \wedge \overline{(I_1 \wedge I_2)}. \quad (13)$$

This implementation uses only seven gates (17 species), which is the minimum number of AND and NOT gates necessary to construct an XOR. Fig. 10 shows that this model is closer to a classical XOR gate than the previous mechanism, given that the output concentration in the region where $I_1 = I_2 \approx 10.0$ units is near 0. The effect of the NOT/AND mismatching is not as pronounced here because of the reduced and asymmetric usage of NOT gates.

The results of a simulation, where the kinetics of a network such as that described by Eq. 13 is constructed so that the transition regions for its component gates are allowed to be relatively gradual, show that despite the seeming nonstandard behavior of the component gates, the XOR function is still properly realized albeit as a smoother function (data not shown). The dynamic range of the output is reduced, however, because of the decreased usage of the full possible transition range of the mechanisms of the individual gates. The output regions in between the extreme points can be thought of as representing partial truth values similar to the behavior of so-called fuzzy logic functions (Klir and Folger, 1988). (See Appendix A.) Such gates may be used to control a smooth transition between two exclusive operating modes of a biochemical pathway. The intermediate truth values then allow the partial activity of both modes of the pathway.

The reaction mechanisms described in the section are built to demonstrate that simple enzymatic networks can represent logic functions that properly execute the truth-table expected by analysis of the connection topology. Despite the fact that each of the gates is continuous over an interval of concentrations instead of being limited to one of two values (0 and 1), networks of these biochemical mechanisms still realize recognizable logic functions. However, these functions must be considered as a generalization of classical Boolean logic into the continuous regime. In the examples in this subsection we considered biochemical gates with relatively simple kinetics. In the next section the simple mechanism that realizes an AND gate (Fig. 6) is reconstructed with rate laws derived from experimental observations of the hexose-phosphate interconversion reactions from glycolysis.

ANALYSIS OF A PORTION OF GLYCOLYSIS

Computational functions in glycolysis

Fig. 11 shows an important control point in the well known BRN of glycolysis/gluconeogenesis that exhibits a structure

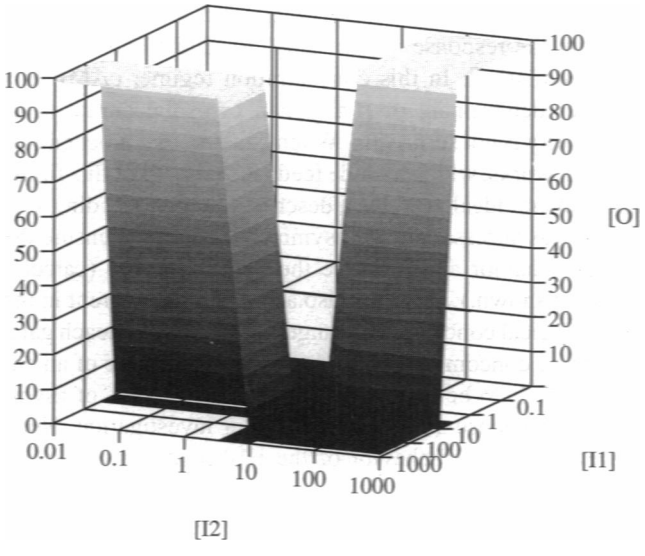

FIGURE 10 Plot of the steady-state concentration of the output of the seven gate XOR network specified in Eq. 13. The choice of the kinetic parameters for the AND and NOT gates is described in Networks of Enzymatic Reaction Mechanisms Implementing Logic Functions. Unlike the mechanism which produced Fig. 5, this mechanism does not violate the XOR at the point $I_1 = I_2 = 10$ units.

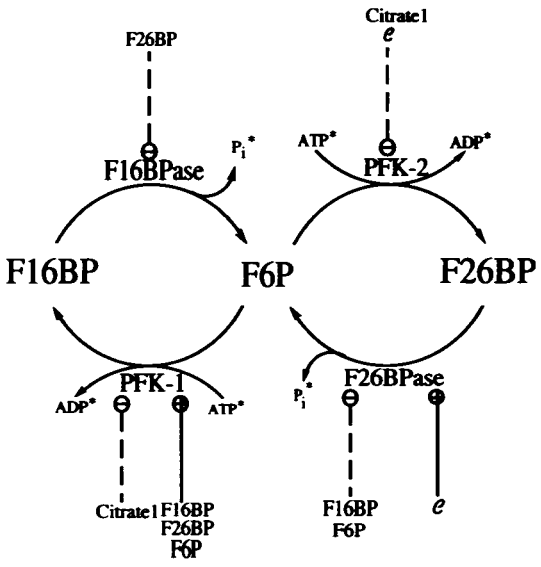

FIGURE 11 Interconversion of fructose 6-phosphate with fructose 1,6-bisphosphate and fructose 2,6-bisphosphate. Species marked by asterisks are considered to be held at constant concentration by buffering or flows. Positive (negative) effectors are connected to their enzymes by a line ending with a circle in which there is a plus (minus) sign.

similar to the mechanism in Fig. 6, for which we showed the property of a logical AND gate. Here, F6P is interconverted between its two bisphosphate forms by specific kinases and phosphatases. The enzymes in this kinetic mechanism are under the allosteric control of many of the chemical signals of cellular energy status such as the adenosine phosphates, cAMP, citrate, and NAD. In general, the gluconeogenic pathway is active under the physiological conditions of low blood glucose, high lactate, adequate three-carbon intermediates for the TCA cycle, and active pathways for fatty acid and glycogen degradation. High lactate and the ready availability of TCA intermediates leads to a flux from the TCA cycle and pyruvate to PEP, which tends to drive the pathway flux in the direction of gluconeogenesis. An abundance of three-carbon fragments also leads to an increased export of mitochondrial citrate to the cytosol. An increase in cytosolic citrate decreases the activity of phosphofructokinase-1 (PFK1) and thus the glycolytic flux from F6P to F16BP.

The concentration of cAMP, the major activator of protein kinase, increases in response to low blood glucose via the glucagon cascade. cAMP-dependent protein kinase and then phosphorylates key enzymes thereby changing their activities and activating glycogen degradation and gluconeogenesis. For example, protein kinase converts F26BPase, the enzyme responsible for the conversion of fructose-2,6-bisphosphate (F26BP) to F6P, to its more active form while reciprocally affecting the activity of phosphofructokinase-2 (PFK2), which accomplishes the reverse reaction. Because F26BP is a potent positive effector of PFK1, the resultant decrease in F26BP reduces the flux from F6P to F16BP. In vivo, the net effect of a change in the levels of both cAMP and cytosolic citrate from low to high concentration is, therefore, a switch of the flux in the metabolic pathway from the direction of glycolysis to that of gluconeogenesis.

We select two of the many possible effectors of PFK1 and PFK2 as the inputs to our proposed device: 1) cytosolic citrate, a potent negative effector of PFK1 whose presence may signal adequate fuel for the TCA cycle, and 2) cAMP, a signal of low blood glucose that stimulates the release of $\mathscr{C}$, the catalytic subunit of cAMP-dependent protein kinase. $\mathscr{C}$ converts PFK2 to its less active, and F26BPase to its more active, form. The kinetic models for these reactions are either based on previous models or experimental data found in the literature. A list of references for all the enzymatic rate laws used in this model and the ones in the next section is given in Tables 1 and 2. The models are based either on variants of the Monod-Wyman-Changeux multieffector allosteric model (Fersht, 1985) or on Cleland-type equations (Cleland, 1963), which are derived from the King-Altman steady-state procedure (King and Altman, 1956). Following the results in earlier subsections (see Implementation of Logic Functions by Multi-Enzyme Mechanisms and Dependence of Functionality on the Exact Kinetic Parameters), we expect the fructose-phosphate interconversion mechanism to function as a logical AND gate similar to the results shown in Fig. 3 or as a more general aggregation such as that shown in Fig. 7.

Comparison with the abstract mechanism

Although the mechanism shown in Fig. 11 has a reaction topology similar to the abstract four-enzyme AND gate shown in Fig. 6, the physiological control of the hexose phosphate gate is somewhat different. In the abstract gate (Eqs. 6–8) the inhibitors block the conversion of species A into one of two equivalent chemical reservoirs, the pools of species B or C. When either E_1 or E_2 is inhibited then the concentration of either C or B, respectively, is increased. It is only when both enzymes are inhibited that most of the material gets converted to A. However, in the hexose-phosphate interconversion mechanism, inhibition of the PFK2 reaction changes the concentration of F26BP only by a small negative amount that, however, is sufficient to deactivate strongly PFK1, and thus material is shunted from F16BP to F6P. There is, therefore, functionally only one reservoir of material into which F6P may be converted in this mechanism (F16BP) versus two in the more abstract case (both F16BP and F26BP).

Calculation of the steady-state behavior of the HIP model

Fig. 12 shows the calculated steady-state surface based on the model of the hexose-phosphate system shown in Fig. 11. The values of the inputs are identical to those employed in the full model described in the next section. In addition the total concentration of fructose-phosphate (25 μM) is set to be consistent with the GGTCA model described below and to correspond roughly with the known physiological concentrations of the sugars (see Table 3). Though the surface is very smooth it is clear that [F6P] is maximized only when both cytosolic citrate (cit 1) and cAMP are high. However, like the gate in Fig. 7, [F6P] deviates significantly from its basal value when one or the other input alone is high. In addition the response of the "gate" to citrate and cAMP is not symmetrical. In this concentration regime, cAMP is a stronger determinant of [F6P] than cytosolic citrate. This asymmetry is not surprising. When constructing biochemical logic networks, which include feedback (e.g., as in flip-flops) from several idealized gates, described in the preceding section, it was necessary to use asymmetrical gates to ensure the proper behavior and preserve the dynamic range (calculations not shown.) There are also asymmetries inherent in the physiological concentration ranges of the inputs to each gate, and thus a concomitant asymmetric input response of an enzyme gate is to be expected. The uses and effects of asymmetrical response are topics for further investigation. Note, however, that the behavior of the HIP model is consistent with the all axioms of fuzzy aggregation described in Appendix A except the optional requirement for symmetry. Further, as would be expected in a fuzzy AND gate, the action of the two inputs is synergetic. The presence of one increases the effectiveness of the other at raising the concentration of F6P. Further, the contour plot on the base of Fig. 12 can be interpreted qualitatively as expressing a combination of those in Figs. 3 and 4, where the output species concentration rises only very gradually through the transition. Following the

TABLE 1 Catalog of reactions and flows used in the GGTCA described in the text and in Figs. 13 and 14

No.	Enzyme	Substrates	Products	Effectors		Kinetics	Source	Reference
1	G C	Glucose0	Glucose1	Mhpt	⊗	D	PI	(Achs et al., 1991)
2	G Dg	Glucose1				C	Arb	
3	GK	Glucose1	G6P			H	PI	(Achs et al., 1991)
		$MgATP^{2-}$	$MgADP^{2-}$					
4	HK	Glucose1	G6P	G6P	⊗	J	PI	*ibid.*
		$MgATP^{2-}$	$MgADP^{2-}$					
		G6P	Gluc1	P_i	⊗			
5	G6Pase			Cit1	⊗	F	RL	*ibid.*
				Gluc1	⊗			
6	PH1	G6P	F6P			P	P1	*ibid.*
		F6P	F16BP	Cit1	⊗			
		$MgATP^{2-}$	$MgADP^{2-}$	AMP	⊕			
7	PFK1			$MgADP^{2-}$	⊕	X	Y	(Eschrich et al., 1990)
				F26BP	⊕			
				F16BP	⊗			
8	F16BPase	Mg^{2+}	F6P	AMP	⊗	H	RL	(Liu et al., 1990)
		F16BP		F26BP	⊗			
		$MgATP^{2-}$	$MgADP^{2-}$	Cit1	⊗			
9	PFK2	6P	F26BP	PEP	⊗	L	CL	(Schaftingen et al., 1986)
				$\mathscr{E}$	⊗			
10	F26BPase	F26BP	F6P	F6P	⊗	X	RL	(Frenze et al., 1990)
				F16BP	⊗			
				$\mathscr{E}$	⊕			
11	Aldolase	F16BP	DHP			S	P1	(Achs et al., 1991)
			GAP					
12		NAD1	NADH1					(Achs et al., 1971)
13	α-GP Dg	α-GP				A	Arb	
14	TPI	DHP	GAP	P_i	⊗	Q	PI	(Achs et al., 1991)
		GAP	13DPGA			W	PI	
15	GAP DH	NAD1	NADH1					*ibid.*
		P_i						
16	PGK	$MgATP^{2-}$	$MgADP^{2-}$			T	PI	*ibid.*
		13DPGA	3-PGA					
17	PGM	3-PGA	2-PGA	23DPGA	⊕	R	RL	(Achs et al., 1971)
18	Enolase	2-PGA	PEP	3-PGA	⊗	Q	PI	(Achs et al., 1991)
				P_i	⊗			
19	PyrK	$MgADP^{2-}$	$MgATP^{2-}$	F16BP	⊕	I	PI	*ibid.*
		PEP	Pyr					
		$MgATP^{2-}$	$MgADP^{2-}$	$MgADP^{2-}$	⊗			
20	PyrC	Pyr	OAA1	P_i	⊗	N	PL	(Warren et al., 1974)
		HCO_3^-	P_i					
21	PEPCK	$MgATP^{2-}$	$MgADP^{2-}$	$MgADP^{2-}$	⊗	K	Y	(Jabalquinto et al., 1993)
		OAA1	PEP	PEP	⊗			
		H^+						
22	Lac DH	NADH1	NAD1			W	PI	(Achs et al., 1991)
		Pyr	Lac					
23	Lac Dg	Lac				A	Arb	

Mechanism notation: *A*, Unimolecular mass action; *B*, Fast mass action (used for fast equilibria, e.g., ionic equilibria); *C*, Michaelis-Menten (MM); *D*, MM with competitive inhibition; *E*, MM with noncompetitive inhibition; *F*, MM with mixed inhibition; *G*, Allosteric MM; *H*, Rapid-equilibrium bi-substrate MM (REBSMM); *I*, REBSMM with an activator; *J*; REBSMM with competitive inhibition; *K*, REBSMM with dead-end competitive inhibition; *L*, REBSMM with noncompetitive inhibition; *M*, Dead-end competitive inhibition of ping-pong bi-bi kinetics; *N*, Rapid-equilibrium ternary MM; *O*, Ternary multisite ping-pong with [P] = 0.0; *P*, Rapid-equilibrium Uni-uni (UU); *Q*, UU with competitive inhibition (UUCI); *R*, UUCI with an activator; *S*, Rapid-equilibrium bi-uni; *T*, Rapid-equilibrium bi-bi; *U*, iso-ordered bi-bi; *V*, ping-pong bi-bi; *W*, Rapid-equilibrium ternary-bi; and *X*, modified Monod-Wyman-Changeux model. The symbol ⊕ (⊗) implies that the preceding effector is an activator (inhibitor) of the relevant enzyme. The abbreviations for the sources are: PI, pancreatic islets; RL, rat liver; PL, pig liver; CL, chicken liver; Y, yeast; Arb, Arbitrarily determined.

discussion in the subsection Connections of Reaction Mechanisms with Computational Functions, we see that the functionality of the gate depends on to what it is connected in situ. This point is more fully addressed in the next section.

In both this model and the ones described in the preceding section, the gates are essentially closed systems in which the total amount of all the relevant substrates is conserved. (We assume implicitly that levels of ATP and ADP are constant and are thus driving the PFK1 and PFK2 reaction away from F6P. This is necessary to ensure that assumption of the irreversibility of the enzyme reaction is reasonable. The system is then formally open to buffered flows of ATP and ADP.) The effects of opening such systems to the inflow and outflow of the hexose-phosphates are discussed in the next section.

ANALYSIS OF A PORTION OF GLYCOLYSIS EMBEDDED IN A LARGE METABOLIC MODEL

The GGTCA model

Figs. 13 and 14 show the metabolic reaction mechanism of glycolysis/gluconeogenesis (GG) coupled to the mitochondrial tricarboxylic acid (TCA) cycle. We have constructed a

TABLE 2 Catalog of reactions and flows used in the GGTCA model described in the text and in Figs. 13 and 14

No.	Enzyme	Substrates	Products	Effectors		Kinetics	Source	Reference
24	CarbA	CO_2	H_2CO_3			C	???	(Fersht, 1985)
25	Cit1Dg	Cit1				C	Arb	
		CoA	ACoA					
26	PyrDHC	NAD2	NADH2			O	Dd	(Wright et al., 1992)
		Pyr						
27	CitSyn	ACoA	Cit2	CoA	⊗	M	"	*ibid.*
		OAA2						
28	Aconitase	Cit2	IC			C	Arb	
29	ICDH	IC	2-KG	NADH2	⊗	M	Dd	(Wright et al., 1992)
		NAD2	NADH2					
30	GluDH	Glu	2-KG	NADH2	⊗	M	"	*ibid.*
		NAD2	NADH2					
		2-KG	Suc					
31	2-KGDHC	NAD2	NADH2			O	"	*ibid.*
		CoA						
32	SucDH	Suc	Fum			P	"	*ibid.*
33	Fumarase	Fum	Mal			P	"	*ibid.*
34	MalE	Malate	Pyr	Asp	⊗	G	"	*ibid.*
35	MalDH	Mal	OAA1			U	"	*ibid.*
		NAD2	NADH2					
36	AspTA	2-KG	Glu			V	"	*ibid.*
		Asp	OAA1					
37	AlaTA	2-KG	Glu			V	"	*ibid.*
		Ala	Pyr					
38	Ala→Pyr	Ala	Pyr			A	"	*ibid.*
39	OAA1→Asp	OAA1	Asp			A	"	*ibid.*
40	Asp→OAA1	Asp	OAA1			A	"	*ibid.*
41	OAA1→OAA2	OAA1	OAA2			A	"	*ibid.*
42	Asp→OAA2	Asp	OAA2			A	"	*ibid.*
43	Suc→Glu	Suc	Glu			A	"	*ibid.*
44	Cit2→Cit1	Cit2	Cit1			C	RL	(Glerum et al., 1990)
45	AK	ADP^{4-}	AMP			B	Arb	
		$MgADP^{2-}$	$MgATP^{2-}$					

Abbreviations are as in Table 1. The abbreviation, Dd, stands for the slime mold *Dictyostelium discoideum*. Most of the rate laws for the TCA cycle (enzymes 26–43) are taken directly from Wright et al. (1992).

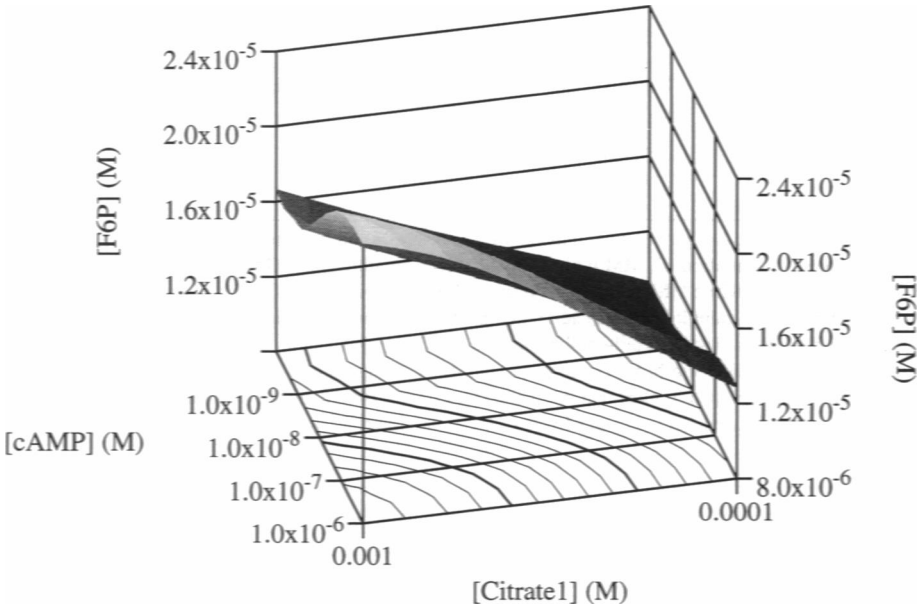

FIGURE 12 Plot of the results of a calculation of the steady-state concentration of Fructose-6-phosphate for the system shown in Fig. 11. The enzyme models are either based on Michaelis-Menten formalisms or modifications of MWC multiple allosteric effector equations. The gate exhibits a function with both AND and OR properties. At low concentrations of both inputs, the mechanism functions similarly to an OR gate while at simultaneously high concentrations of the input species (Citrate1 and cAMP), the output behavior more closely resembles a fuzzy-logic AND gate. The mechanism, like the more abstract gate (Fig. 6) which produced the results shown in Fig. 7, satisfies the requirements for a fuzzy aggregation function.

computer model (GGTCA) of this system that contains 58 reactions dependent on 57 chemical species. The rate laws for each of the enzymatic steps are mostly taken directly from the literature (see Tables 1 and 2.) In a few cases, the rate laws were slightly modified to take into account interactions with other known effectors, or were postulated *ad hoc* to produce physiologically reasonable behavior of the intermediate concentrations. The mathematical specification of the model is not included here because of space limitations; however, it may be obtained by writing to the authors. The hexose-

TABLE 3 Comparison of calculated steady-state concentrations of the species in the GGTCA model with experimentally observed concentration ranges where available

Species	Glycolytic	Gluconeogenic	Experimental	Reference
Blood Glucose	4.00 mM	4.00 mM	4.4–6.6 mM	(Stryer, 1988)
Glucose (cytosolic)	392.44 μM	403.35 μM		
G6P	27.5 μM	63.63 μM	50–261 μM	(Achs et al., 1971)
F6P	7.65 μM	17.84 μM	14.5–65.5 μM	*ibid.*
F26BP	1.27 μM	11.65 nM	0.5–3.0 μM	*ibid.*
F16BP	2.08 μM	1.026 μM	6.4–19.2 μM	*ibid.*
DHP	56.90 μM	47.26 μM	23.2–43.6 μM	*ibid.*
Glycerol Phosphate	9.84 μM	8.20 μM		
GAP	6.31 μM	5.247 μM	2.75–6.75 μM	*ibid.*
13DPGA	278.15 nM	357.87 nM	440–2040 μM	*ibid.*
PGA3	316.66 μM	407.69 μM	186–1340 μM	*ibid.*
PGA2	62.77 μM	81.84 μM	28.0–148.0 μM	*ibid.*
PEP	94.07 μM	124.02 μM	107.0–807 μM	*ibid.*
Pyruvate	24.63 μM	1.25 mM	11.0–55.0 μM	(Achs and Garfinkel, 1977)
Lactate	2.32 μM	2.32 μM	1.0–7.7 mM	*ibid.*
Citrate 1	105.44 μM	637.78 μM	52–2765 μM	(Achs et al., 1971)
23DPGA	1.00 μM	1.00 μM	0.04–1.88 μM	*ibid.*
Alanine	2.38 mM	5.43 mM		
Aspartate	2.89 mM	1.75 mM		
Oxalacetate 1	4.47 μM	2.43 μM		
Oxalacetate 2	2.50 μM	2.51 μM		
CoA	100.00 μM	100.00 μM		
ACoA	11.56 μM	83.69 μM		
Citrate 2	41.87 μM	48.39 μM		
Isocitrate	9.758 μM	10.03 μM		
2-Ketoglutarate	7.28 μM	10.57 μM		
Glutamate	7.96 mM	5.49 mM		
Succinate	699.42 μM	814.66 μM		
Fumarate	38.85 μM	40.15 μM		
Malate	213.47 μM	220.96 μM		
Pα	90%	103%		
H^+	39.81 nM	39.81 nM		
P_i	100.00 μM	100.00 μM		
Mg	874.32 μM	874.32 μM		
ATP	87.70 μM	87.70 μM		
AMP	500.00 μM	500.00 μM		
ADP	624.33 μM	624.33 μM		
MgATP	3.07 mM	3.07 mM		
MgADP	1.09 mM	1.09 mM		
MgAMP	26.27 μM	26.27 μM		
HATP	22.03 μM	22.03 μM		
HADP	156.82 μM	156.82 μM		
HAMP	61.44 μM	61.44 μM		
cAMP	100.00 pM	1.0 μM		
NAD1	3.00 mM	3.00 mM		
NADH1	100.00 nM	100.00 nM		
NAD2	72.00 μM	72.00 μM		
NADH2	180.00 μM	180.00 μM		
CO_2	765.26 nM	856.92 nM		
CO_3	5.78 nM	6.47 nM		
HCO_3	4.917 μM	5.51 μM		
H_2CO_3	491.76 nM	550.67 nM		
PT	440.00 nM	440.00 nM		
C0	1.51 pM	8.30 nM		
PFbar	9.53 μM	36.32 nM		
PFphi	467.85 nM	9.96 μM		

The column labeled "Glycolytic Concentrations" contains the concentrations of the metabolites when the flow of ACoA and the concentration of cAMP are at their lowest values and the flux through the pathway is in the glycolytic direction. The column labeled "Gluconeogenic Flux" contains metabolite concentrations obtained when ACoA flow and cAMP concentration are at their highest values (during the calculation) and the mode of the pathway has switched to gluconeogenesis. All experimental values must be considered as estimates only, as many were read from graphs or are indirectly calculated using other measured concentrations. The basal rate of flow of ACoA is 0.46 mM/min as is assumed by Wright et al. (1992).

phosphate "gate" discussed in the preceding section (and shown in Fig. 11) appears as a set of reactions early in the glycolytic pathway. Because this model exhibits a large number of regulatory interactions the "logic" governing control of the network may be very complex. We wish to find what computations, if any, are performed by the hexose phosphate interconversion mechanism within the larger BRN. We determine how the logical structure of the steady-state surface of the mechanism discussed in the last section changes when placed within such a large network. The GGTCA model includes a number of externally controlled chemical species that affect the dynamics of the network and sub-

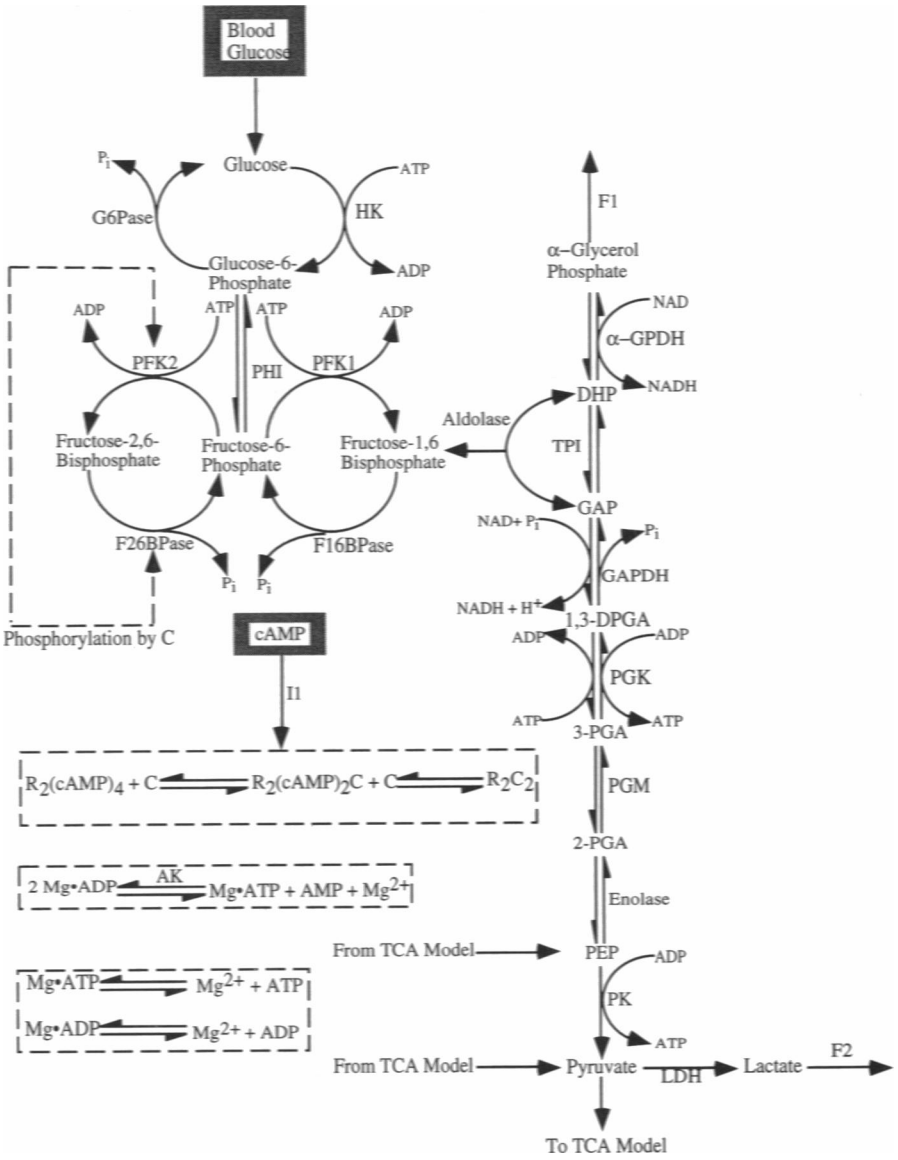

FIGURE 13 A map of the glycolytic/gluconeogenic pathway modeled in the GGTCA model described in the text. Here and in Fig. 14, external inputs to the network are in grey stippled boxes. See footnote 1 for abbreviations. cAMP is chosen as one of the external inputs to the network. This model is connected to the TCA model in Fig. 14.

sequently the steady-state values of all the flows and chemical concentrations.

For our initial study of this model, we choose the two inputs to be: 1) the rate of flow of acetyl-CoA into the system, expressed as a percentage of the basal flow, P_α, and 2) cAMP concentration. For a number of species we hold the concentration constant. These include: extracellular glucose, cytosolic AMP, inorganic phosphate (p_i), mannoheptulose, coenzyme-A, 2,3-bisphosphoglycerate, pH, and cytosolic and mitochondrial NAD and NADH. In addition, the total adenine nucleotide and magnesium concentrations are conserved. The concentrations of these species are set so that they approximate the physiological state of the network close to a switch from glycolysis to gluconeogenesis. To construct the steady-state surfaces shown in Figs. 15 and 16, the two inputs, P_α and cAMP, are varied between their physiological extremes and the steady-state of the network is found as described in Materials and Methods. Examination of Fig. 14 shows that an increase in P_α results in an increased transport of mitochondrial citrate into the cytosol. cAMP shifts the equilibrium of cAMP-dependent protein kinase toward the liberation of its catalytic subunit (Fig. 13). In the calculations described here, the ranges of concentrations of cytosolic citrate and $\mathscr{E}$ are identical to those used in the preceding section.

Calculation of the steady-state behavior of the GGTCA model

Fig. 15 shows the stationary-state concentration of F6P as a function of P_α and cAMP. The results are very similar to those obtained in the HIP model described above. The embedded mechanism functions as a highly smoothed version of Fig. 3 and has properties somewhere between an AND and an OR gate (as in Fig. 7). Again, the response of [F6P] to the two inputs is asymmetric although perhaps slightly less so

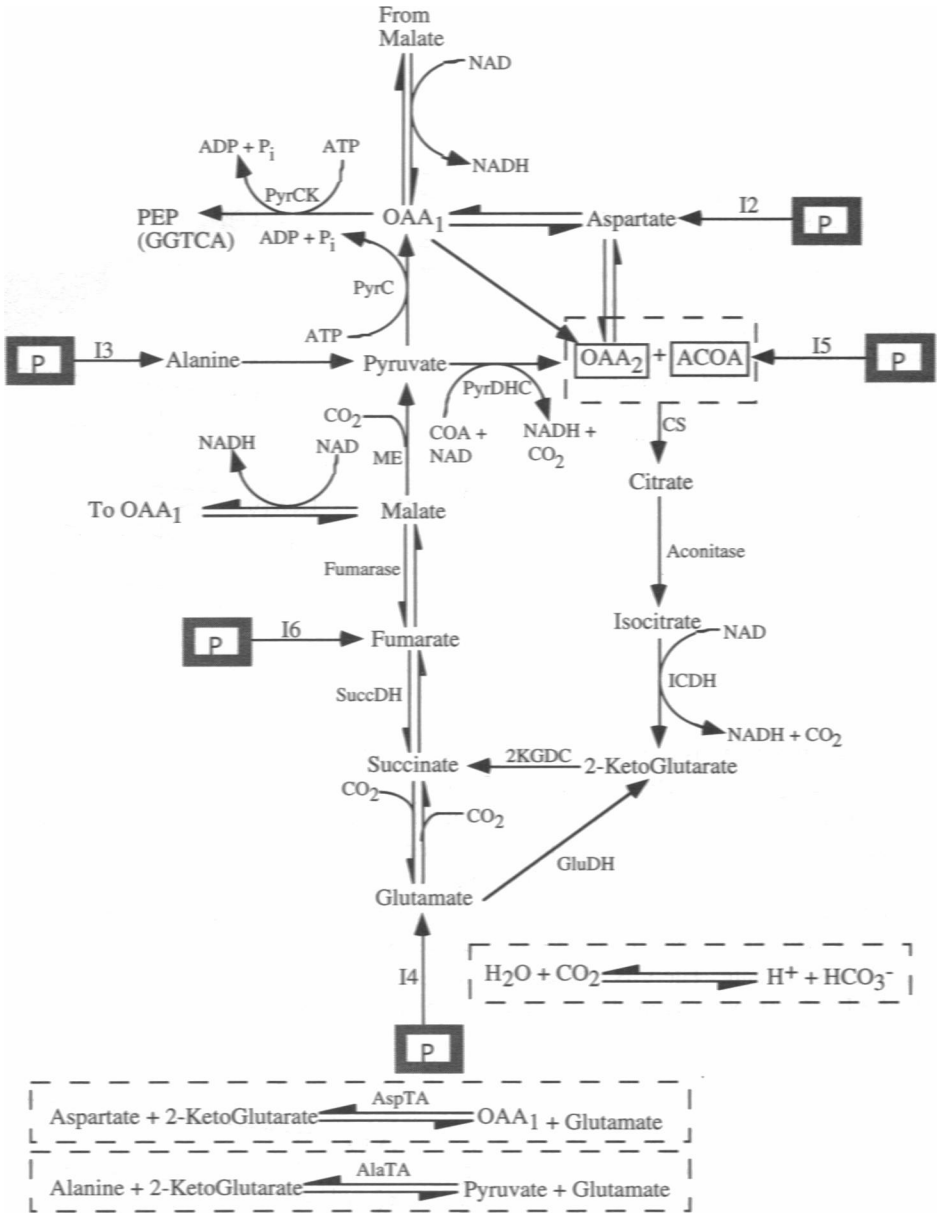

FIGURE 14 A map of the TCA Cycle as modeled in the GGTCA simulations. This portion of the model is taken almost *in toto* from the model in references (Wright, Butler, and Albe, 1992) and (Albe and Wright, 1992). The symbol, 'P', stands for external protein (amino acid) inputs. We chose the input of ACOA (I_5 in the diagram) to be the other input to the glycolysis system. Note that arrows pointing to and away from the box surrounding OAA2 and ACOA indicate production or consumption of the two species respectively.

than in Fig. 12. The qualitative behavior of the HIP mechanism is, however, unchanged by its placement within the larger network.

The GGTCA model shows a switching from glycolytic to gluconeogenic flux over this range of input concentrations. Fig. 16 shows the flux through the glucose carrier protein (fGCP), which is modeled as a reversible enzyme that transports extracellular to cellular glucose and back. When it is negative, glucose is being consumed by the pathway, and when it is positive, glucose is being produced. Glycolysis dominates the pathway only when all the individual fluxes between the pathway intermediates point in the right direction. In this case, these fluxes follow the behavior of fGCP very closely. This switch, from negative to positive flux, occurs only when both P_α and cAMP are significantly greater than their basal values (basal values: $P_\alpha = 0.90$, [cAMP] = 0.1 nM, switch point: $P_\alpha > 0.989$, [cAMP] > 10.0 nM). The hexose interconversion pathway, embedded in the GGTCA mechanism, acts as a type of smooth AND gate that effects a switching between glycolytic and gluconeogenic flux only when both the indicators of low blood glucose and sufficient fuel for the TCA cycle are high.

DISCUSSION AND CONCLUSIONS

We have shown that the macroscopic kinetics of certain enzyme reaction mechanisms have properties analogous to logic functions. These functions can be classical, following the axioms of Boolean logic, or they may implement a more general class of logic called fuzzy logic. For example, different choices of the kinetic parameters (e.g., V_{max}, K_I, etc.) of the mechanism in Fig. 6 can realize either a reasonably

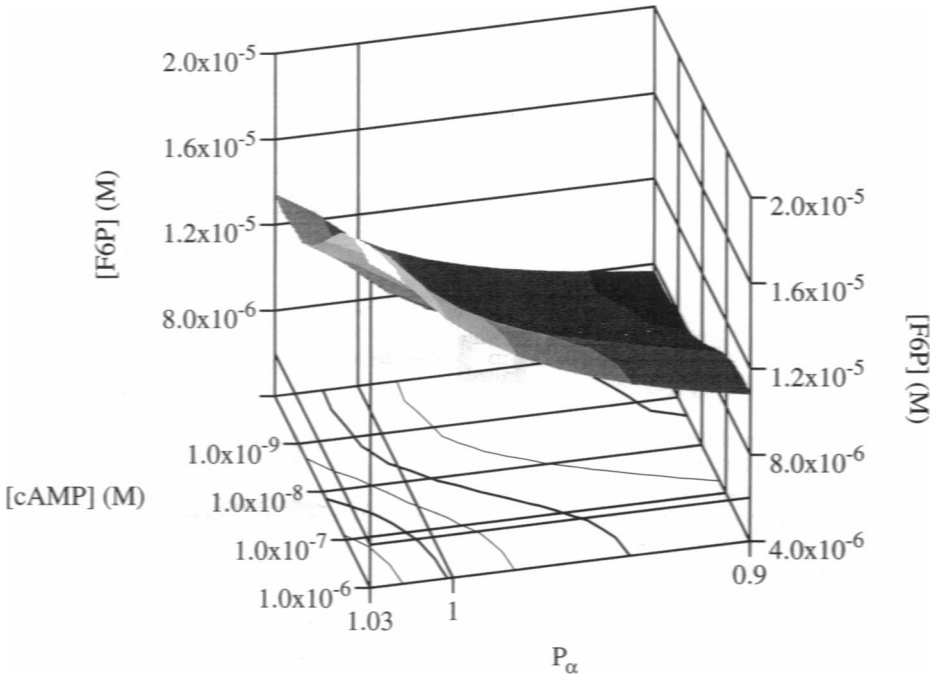

FIGURE 15 Plot of the steady-state concentration of Fructose-6-phosphate as a function of P_α (proportional to the rate of flow of acetyl-coenzyme A into the TCA cycle) and cAMP. This calculation is the result of an integration of the hexose-phosphate interconversion pathway embedded in the GGTCA model (see text). Note that though the absolute concentrations of F6P are different than those in Fig. 12, the overall shape of the surface is very similar. The mechanism functions as a fuzzy logic aggregation function akin to the fuzzy AND gate.

crisp AND function (as in Fig. 3), a fuzzy AND function, or a fuzzy aggregation function (as in Fig. 7). The last case is interesting in that there are two distinct functionalities depending on the concentration regime of the inputs. If the concentration of either I_1 or I_2 is below approximately 0.1 units, then the mechanism functions like an OR gate. If both inputs are above 0.1 units, then the gate behaves as a nearly classical AND gate. There is, therefore, more than simply ON/OFF information encoded in the interaction between the fuzzy-logic "gate" mechanism and its inputs. Fuzzy logic, and the closely related fields of multivalued (Schaerf, 1991) and continuous logic (Levin, 1990a, b), have only recently become the focus of research in engineering and computer science. They have become important in pattern recognition algorithms and in the field of knowledge representation where it is used when there is contradictory information about a proposition, or there is uncertainty in the data. It has also been argued that multivalued and continuous logic may

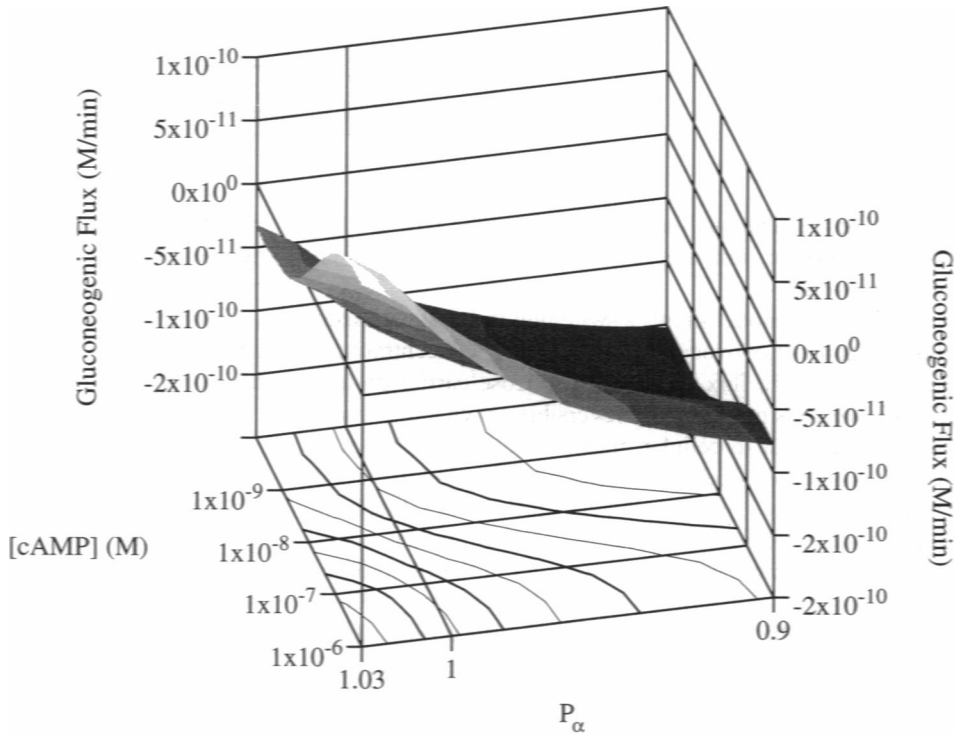

FIGURE 16 Plot of the net flow from blood glucose to cytosolic glucose (as measured by the flux through the glucose carrier protein) as a function of the P_α and cAMP levels (designated as "Gluconeogenic Flux"). A positive flux indicates that gluconeogenesis is active and a negative flux indicates glycolysis. The fluxes through the reversible enzymes PHI, aldolase, TPI, GAPDH, PGK, PGM and enolase also switch within this regime. The switch from positive to negative flux only occurs when both P_α and cAMP are significantly different from their basal levels (positive flux in the region bounded by ($P_\alpha \approx 0.99$, cAMP ≈ 0.16 μm) and ($P_\alpha \approx 1.03$, cAMP ≈ 10.0 nm)). In order to achieve switching, other chemical species whose concentrations correlate with the energetic requirements of the cell (e.g. NAD, NADH, AMP, p_i, lactate, etc.) have been set to the values they would have during a physiological change from glycolysis to gluconeogenesis.

allow for a larger bandwidth for information transmission than the familiar two-valued logic.

Second, we have shown by example that the kinetics of a portion of a well established BRN can carry out a computational function; the example is the hexose-phosphate interconversion pathway embedded in a comprehensive model of glycolysis/gluconeogenesis coupled to the tricarboxylic acid cycle. The HIP pathway, consisting of the three fructose-phosphate forms, the four interconversion enzymes, and under the external control of cAMP and cytosolic citrate, functions as a fuzzy aggregation operator in concentration as well as in flux.

The switching between glycolysis and gluconeogenesis is controlled by many interrelated and not necessarily consistent chemical indicators of cellular energy status (e.g., the TCA cycle does not necessarily have a surfeit of intermediates only when blood glucose is low). As such, the metabolic HIP switch must be able to determine an efficient switch point in the face of somewhat "contradictory" information. It is reasonable, therefore, to expect that the logic that governs the change in pathway flux from glycolysis to gluconeogenesis, when there is both enough energy to drive respiration and not enough blood glucose, is a switch but with a "fuzzy" transition.

Having shown that macroscopic kinetics may have computational functions we may invert the purpose of the investigation. We may ask what methods of testing for logic functions, as in electronic circuit theory, may be applicable to the investigation of complex reaction mechanisms. It is useful to construct truth-tables, obtained from experiments on a given reaction mechanism in which, for example, an increase in the concentration of any two or more reactants produces an increase or decrease in the concentration of a third reactant (or product). Both probabalistic reconstruction analysis and dependency analysis (Conant, 1988a, b) are other examples of systems analysis techniques that may be applied to experimental observations of interdependencies between the concentrations of chemical species in order to reconstruct complex reaction mechanisms. We address these issues in a separate study.

We thank Dr. Lubert Stryer for many useful discussions and suggestions. This work was supported in part by the National Science Foundation and the National Institutes of Health. A.P.A. was also supported, in part, by the National Institute of Mental Health grant no. MH 45324.

APPENDIX A: SOME AXIOMS OF FUZZY LOGIC

The axioms of fuzzy logic (Klir and Folger, 1988) are based on the use of fuzzy membership functions, $\mu_{\mathcal{A}}(\mathcal{C})$ which are an (often arbitrary) measure of the belonging of a given object, $\mathcal{C}$, to a given set, $\mathcal{A}$, i.e., it measures how true the defining characteristic of the set is for the object. For example, if $\mathcal{A}$ = *Old* and the objects are {*2 years old*, *40 years old*, *90 years old*}, then $\mu_{\mathcal{A}}$ might take on the values {0, 0.5, 1.0}, respectively. For comparison, in Boolean (two-valued or crisp) logic, this membership function takes on only the values 0 or 1; an object either belongs to the set or it does not. Most generally, fuzzy logic functions are described as interval mappings,

$$f := [0, 1]^n \leftrightarrow [0, 1]^m. \tag{A1}$$

A fuzzy NOT gate, for example, is defined by the mapping

$$\text{NOT} := [0, 1] \leftrightarrow [0, 1], \tag{A2}$$

where $\text{NOT}(\mu_{\mathcal{A}}(\mathcal{C}))$ maps the membership of objects in $\mathcal{A}$ (e.g., *Old*) to that in the set $\bar{\mathcal{A}}$ (e.g., Young) and follows the following two axioms, which are based on those in Klir and Folger (1988):

Axiom A.1 NOT(0) = 1 and NOT(1) = 0; boundary conditions which also hold for crisp logic.

Axiom A.2 For all $a, b \in [0, 1]$, *if* $a < b$, then $\text{NOT}(a) \geq \text{NOT}(b)$, i.e. NOT is monotonic nonincreasing.

In an actual transistor-transistor logic (TTL) implementation of a crisp logic gate the mapping, Eq. A.1, is not between 0 and 1 but between voltages $V_{\text{ttl low}}$ = 50 mV and $V_{\text{ttl high}}$ = 3.5 V. In order to interface TTL to complementary metal oxide semiconductor, voltage-matching circuitry is required; thus, it is not unreasonable at first to disregard the fact that our biochemical gates map the interval $[a, b]$ to $[c, d]$ instead of that required in Eq. A.1. We assume that the actual input/output values of our gates are evolved to permit proper chemical matching between biochemical subsystems. Therefore, biochemical gates may well functionally satisfy Eq. A.1. With this in mind, the biochemical NOT gate described above satisfies these two fundamental axioms for the fuzzy complement as well as the common ancillary axiom of continuity. It does not, however, necessarily satisfy a requirement for involution, which is sometimes associated with fuzzy complements. This is merely a result of the more general mapping of biochemical gates. The smooth AND gates discussed in earlier sections (Implementation of Logic Functions by Single-Enzyme Mechanisms, and Implementation of Logic Functions by Multi-Enzyme Mechanisms) also satisfy the axiomatic requirements for a fuzzy AND though the requirement for associativity is violated if the biochemical gate has any asymmetry with respect to its inputs. (But see beginning of paragraph.) Further, for certain choices of kinetic parameters it is difficult to ignore the violation of the following fundamental axiom:

Axiom A.3 AND(1, 1) = 1; AND(0, 1) = AND(1, 0) + AND(0, 0) = 0 (Boundary conditions.)

For example, in Fig. 7, $[A]$ is significantly increased by the application of I_1 (I_2) in the absence of I_2 (I_1). In this case, the system is more accurately described as a fuzzy aggregation operator (of which the fuzzy AND and fuzzy OR are special cases)

$$\mathcal{A}: [0, 1]^n \leftrightarrow [0, 1] \tag{A3}$$

which obeys the following axioms:

Axiom A.4 $\mathcal{A}(0, 0, 0, \cdots, 0) = 0$ and $\mathcal{A}(1, 1, 1, \cdots, 1) = 1$.

Axiom A.5 $\mathcal{A}$ is monotonic nondecreasing in all its arguments.

Axiom A.6 $\mathcal{A}$ is a continuous function.

There is another auxiliary axiom which is not necessary but often included:

Axiom A.7 $\mathcal{A}$ is a symmetric function in all its arguments.

The gate that produced Fig. 7 satisfies this requirement, but in general, biochemical gates are asymmetric. In fact, it is difficult to analyze the logical consequences of input response asymmetry in real biochemical gates since both the gate's sensitivity to a given effector and the physiological concentration range of the effector are relevant.

REFERENCES

Acerenza, L., H. M. Sauro, and H. Kacser. 1989. Control analysis of time-dependent metabolic systems. *J. Theor. Biol.* 137:423–444.

Achs, M. J., J. H. Anderson, and D. Garfinkle. 1971. Gluconeogenesis in rat liver cytosol. I. Computer analysis of experimental data. *Comput. Biomed. Res.* 4:65–106.

Achs, M. J., and D. Garfinkel. 1977. Computer simulation of energy metabolism in anoxic perfused rat heart. *Amer. J. Physiol.* 232:(5) R164–R174.

Achs, M. J., L. Garfinkel, and D. Garfinkle. 1991. A computer model of pancreatic islet glycolysis. *J. Theor. Biol.* 150:109–135.

Albe, K. R., B. E. and Wright. 1992. Systems analysis of the tricarboxylic acid cycle in *Dictyostelium discoideum*. *I. Control analysis. J. Biol. Chem.* 267:3106–3114.

Cleland, W. W. 1963. The kinetics of enzyme-catalyzed reactions with two or more substrates or products. I. Nomenclature and rate Equations. *Biochem. Biophys. Acta.* 67:104–137.

Conant, R. C. 1988a. Extended dependeacy analysis of large systems. I. Dynamic analysis. *Int. J. Gen. Syst.* 14:97–123.

Conant, R. C. 1988b. Extended depeadeacy analysis of large systems. II. Static analysis. *Int. J. Gen. Syst.* 14:125–141.

Eschrich, K., W. Schellenberger, and E. Hofmann 1990. A hysteretic cycle in glucose 6-phosphate metabolism observed in a cell-free yeast extract. *Eur. J. Biochem.* 188:697–703.

Fersht, A. 1985. Enzyme Structure and Mechanism. W. H. Freeman and Company, New York.

Frenzel, J., W. Schellenberger, K. Eschrich, and E. Hofmann. 1990. Regulation of the fructose 6-phosphate/fructose 2:6-bisphosphate cycle by enzyme phosphorylation and *sn*-glycerol 3-phosphate. *Biol. Chem. Hoppe-Seyler* 371:841–850.

Glass, L., and S. Kauffman. 1973. The logical analysis of continuous nonlinear biochemical control networks. *J. Theor. Biol.* 39:103–129.

Glerum, D. M., D. Claeys, W. Mertens, and A. Azzi. 1990. The tricarboxylate carrier from rat liver mitochondria: purification, reconstitution and kinetic characterization. *Eur. J. Biochem.* 194:681–684.

Goldbeter, A., and D. E. Koshland, Jr. 1981. An amplified New York: sensitivity arising from covalent modification in biological systems. *Proc. Natl. Acad. Sci. USA.* 78:6840–6844.

Hjelmfelt, A., and J. Ross. 1992. Chemical implementation and thermodynamics of collective neural networks. *Proc. Natl. Acad. Sci. USA.* 89: 388–391.

Hjelmfelt, A., and J. Ross. 1993. Mass coupled chemical systems with computational properties. *J. Phys. Chem.* 97:7988–7992.

Hjelmfelt, A., and J. Ross. 1994. Pattern recognition, chaos, and multiplicity in neural networks of excitable systems. *Proc. Natl. Acad. Sci. USA.* 91:63.

Hjelmfelt, A., F. W. Schneider, and J. Ross. 1993. Pattern recognition in coupled chemical kinetic systems. *Science.* 260:335–337.

Hjelmfelt, A., E. D. Weinberger, and J. Ross. 1991. Chemical implementation of neural networks and turing machines. *Proc. Natl. Acad. Sci. USA.* 88:10983–10987.

Hjelmfelt, A., E. D. Weinberger, and J. Ross. 1992. Chemical implementation of finite state machines. *Proc. Natl. Acad. Sci. USA.* 89:383–387.

Horowitz, P., and W. Hill. 1984. The Art of Electronics. Cambridge University Press, New York.

Jabalquinto, A. M., and E. Cardemil. 1993. The kinetic mechanism of yeast phosphoenolpyruvate carboxykinase. *Biochem. Biophys. Acta.* 1161: 85–90.

Kauffman, S. A. 1969. Metabolic stability and epigenesis in randomly constructed genetic nets. *J. Theor. Biol.* 22:437–467.

Kauffman, S. A. 1971. Gene regulation networks: a theory for their global structure and behaviors. *In* A. Moscona and A. Monroy, editors, Current Topics in Developmental Biology. Academic Press, New York. 145–181.

King, E. L., and C. Altman. 1956. A schematic method of deriving the rate laws for enzyme-catalyzed reactions. *J. Phys. Chem.* 60:1375–1378.

Klir, G. J., and T. A. Folger. 1988. Fuzzy Sets, Uncertainty, and Information. Prentice Hall, Englewood Cliffs, New Jersey.

Levin, V. I. 1990a. Continuously-valued logic: generalizations and applications I. *Aut. i Telemek.* 8:3–22.

Levin, V. I. 1990b. Continuously-valued logic: generalizations and applications II. *Aut. i Telemek.* 9:3–26.

Liu, F., and H. J. Fromm. 1990. Kinetic studies on the mechanism and regulation of rabbit liver fructose-1,6-bisphosphatase. *J. Biol. Chem.* 265: 7401–7406.

McCulloch, W. S., and W. Pitts. 1943. A logical calculus of the idea immanent in nervous activity. *Bull. Math. Biophys.* 5:115–133.

Monod, J., and F. Jacob. 1961. General conclusions: teleonomic mechanisms in cellular metabolism, growth and differentiation. *In* Cellular Regulatory Mechanisms. Cold Spring Harbor, New York. 389–401.

Okamoto, M., T. Sakai, and K. Hayashi. 1988. Biochemical switching device: monocyclic enzyme system. *Biotechnol. Bioeng.* 32:527–537.

Roussel, M. R., and S. J. Fraser. 1993. Global analysis of enzyme behavior. *J. Phys. Chem.* 97:8316–8327.

Schacter, E., P. B. Chock, and E. R. Stadtman. 1984a. Energy consumption in phosphorylation/dephosphorylation cascade. *J. Biol. Chem.* 259: 12260–12264.

Schacter, E., P. B. Chock, and E. R. Stadtman. 1984b. Regulation through phosphorylation/dephosphorylation cascade systems. *J. Biol. Chem.* 259: 12252–12259.

Schaerf, M. 1991. Notes on Ginsberg's multivalued logics. *Comput. Intel.* 7:154–159.

Schaftingen, E. v., and H.-G. Hers. 1986. Purification and properties of phosphofructokinase 2/fructose 2:6-bisphosphatase from chicken liver and from pigeon muscle. *Eur. J. Biochem.* 159:359–365.

Stryer, L. 1988. Biochemistry. W. H. Freeman and Company, New York.

Sugita, M. 1963. Functional analysis of chemical systems in vivo using a logical circuit equivalent. II. The idea of a molecular automaton. *J. Theor. Biol.* 4:179–192.

Thomas, R. 1973. Boolean formalization of genetic control circuits. *J. Theor. Biol.* 42:563–585.

Warren, G. B., and K. F. Tipton. 1974. Pig liver pyruvate carboxylase: the reaction pathway for the decarboxylation of oxaloacetate. *Biochem. J.* 139:321–329.

Wright, B. E., M. H. Butler, and K. R. Albe. 1992. Systems analysis of the tricarboxylic acid cycle in *Dictyostelium discoideum*. I. The basis for model construction. *J. Biol. Chem.* 267:3101–3105.